ORGANOMETALLICS

pubs.acs.org/Organometallics Article

Syntheses, Structures, Reactivities, and Dynamic Properties of Gyroscope-like Complexes Consisting of Rh(CO)(X) or $Rh(CO)_2(I)$ Rotators and Cage-like *Trans* Aliphatic Dibridgehead Diphosphine Stators

Alexander L. Estrada, Leyong Wang, Nattamai Bhuvanesh, Frank Hampel, and John A. Gladysz*

Cite This: *Organometallics* 2022, 41, 733−749 Read Online

ABSTRACT: Square planar *trans*-$Rh(CO)(Cl)[P((CH_2)_{14})_3P]$ (**4c**) is prepared from *trans*-$Rh(CO)(Cl)[P((CH_2)_6CH{=}CH_2)_3]_2$ by a C=C metathesis/hydrogenation sequence (41%). Additions of NaBr, NaI, or KSCN give the substitution products *trans*-$Rh(CO)(X)[P((CH_2)_{14})_3P]$ (X = Br/I/−NCS, **5c**/**6c**/**7c**, 97−44%). Additions of $ZnPh_2$, MeLi, or $NaBH_4$ give *trans*-$Rh(CO)(R)[P((CH_2)_{14})_3P]$ (R = Ph/Me, **8c**/**9c**, ∼94−89%) or *trans*-$Rh(CO)(H_2BH_2)[P((CH_2)_{14})_3P]$ (**10c**, 99%). Reactions with $BrCCl_3$ or CO give the octahedral or trigonal bipyramidal addition products *trans*-$Rh(CO)(Cl)(Br)(CCl_3)[P((CH_2)_{14})_3P]$ (**11c**, 97%) or *trans*-$Rh(CO)_2(I)[P((CH_2)_{14})_3P]$ (**12c**, ∼98%). The crystal structures of **5c**, **6c**, **8c**, and **10c** are determined. These and other data are used to calculate the dimensions of the rotators and void spaces of the diphosphine cages, aiding the interpretation of dynamic properties. Specifically, **4c**−**6c** and **9c**−**10c** exhibit a single set of seven CH_2 ^{13}C NMR signals at room temperature, although three sets of seven are expected from symmetry (⇒ facile 360° Rh(CO)(X) rotation); **7c**−**8c** exhibit two sets of seven signals with a ca. 2:1 area ratio (∼90° Rh(CO)(X) rotation); **11c** exhibits three sets of seven signals (no $Rh(CO)(Cl)(Br)(CCl_3)$ rotation). The barrier to $Rh(CO)_2(I)$ rotation in **12c** is bounded as higher than that of Rh(CO)(I) rotation in **6c**, but the rotamers preferentially interconvert via CO dissociation/addition. Reaction of **4c** and excess PMe_3 gives *trans*-$Rh(CO)(Cl)(PMe_3)_2$ (72%) and the dibridgehead diphosphine $P((CH_2)_{14})_3P$ (58%). The latter reacts with $[(OC)_2Rh(\mu\text{-}Cl)]_2$ to regenerate **4c** (58%).

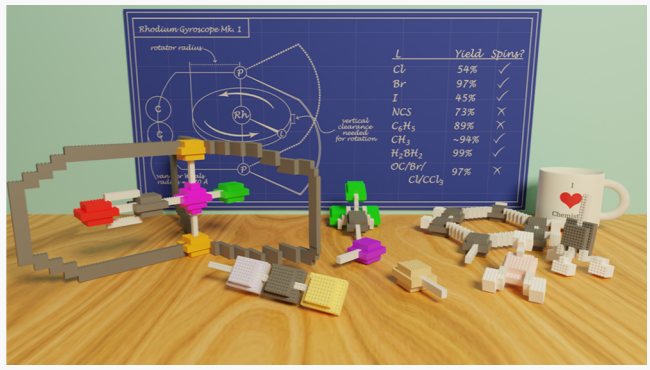

■ INTRODUCTION

There is now an extensive literature of sterically shielded molecular rotors.[1,2] Shielding represents an important design element in any molecular machine or device with a rotating component, much like macroscopic industrial flywheels, gearboxes, and drivebelts, which are normally kept in protective housings.[3] Packaging is also an important consideration for microelectromechanical systems (MEMS), which can have diverse types of moving parts.[4]

We have had a long-standing interest in types of compounds that show promise as molecular gyroscopes.[1b] In particular, we discovered that three-fold intramolecular ring-closing metatheses of coordination complexes with *trans* phosphine ligands of the formula $P((CH_2)_mCH{=}CH_2)_3$ afford, after hydrogenations, the cage-like dibridgehead diphosphine adducts *trans*-$ML_y[P((CH_2)_n)_3P]$ (**I**; Scheme 1), where $n = 2m + 2$. Such sequences can be effected with trigonal bipyramidal ($n \geq 10$),[5] octahedral ($n \geq 14$),[6] and square planar ($n \geq 14$) educts.[7] Depending upon the value of n and the nature of the ligands, the ML_y rotator may be (1) capable of a 360° rotation, (2) capable of a substantial oscillation but not a full 360° rotation, or (3) essentially locked in place. Related species with silicon-(*p*-arylene)-silicon axes as opposed to phosphorus-metal-phosphorus axes have been similarly accessed by Setaka.[2b,8]

The synthesis of a typical square planar system with $n = 14$ and $ML_y = PtCl_2$ is depicted in Scheme 1. The corresponding $PdCl_2$ adduct is similarly available,[7a] and both have an extensive chloride ligand substitution chemistry.[7a,9] Certain

Received: December 21, 2021
Published: February 21, 2022

https://doi.org/10.1021/acs.organomet.1c00708
Organometallics 2022, 41, 733−749

Scheme 1. Synthesis of a Representative Square Planar Group 10 Gyroscope-Like Complex and Displacement/Recomplexation of the Dibridgehead Diphosphine 1c

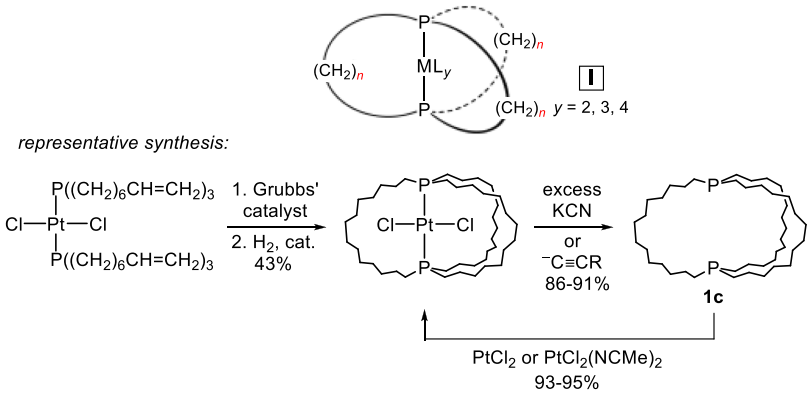

nucleophiles can also displace the dibridgehead diphosphine ligand $P((CH_2)_{14})_3P$ (**1c**). Each of these sixteen-valence-electron species and the $NiCl_2$ analogue can also be accessed from **1c** and MCl_2 sources.[10] Although various mechanistic issues associated with these transformations remain to be clarified, such diphosphines can function as "container molecules" for transporting MX_2 fragments from one medium to another.[10]

While there are many fascinating properties of these group 10 complexes,[7,9] we were also interested in developing isoelectronic group 9 species. Since the two non-phosphine ligands must now supply a total of three valence electrons, they must be unlike, and the rotator will feature a dipole. Dipolar entities are capable of interacting with electric fields, and this represents one approach to driving the unidirectional rotation required for molecular gyroscopes.[1,11] Also, certain group 9 sixteen-valence-electron species are capable of adding suitable Lewis bases to give five coordinate eighteen-valence-electron trigonal bipyramidal adducts,[12] and this represents a possible approach to reversible modulating rotation or "braking".

For this study, we were particularly attracted to rhodium, in part due to the numerous reactions that can be catalyzed by rhodium phosphine complexes and the ease of interconversion of many rhodium(I) and rhodium(III) species.[13] It is of obvious interest to probe the feasibility and selectivity of catalysis within the diphosphine cage. While some of the preceding objectives might be pursued with group 10 adducts, it can be challenging to access unsymmetrically substituted species with dipolar rotators,[9] and there is a narrower range of M(II)/M(IV) couples.

Accordingly, we set out to synthesize and develop the chemistry of Rh(CO)(X) adducts of dibridgehead diphosphines such as **1c**. In this full paper, a variety of such compounds are prepared and structurally characterized. Their dynamic behavior, and those of five and six coordinate derivatives, are probed by variable-temperature NMR. Trends are analyzed in detail, and the feasibility of oxidative addition within the diphosphine cage is established. Portions of this work have been communicated.[14]

■ RESULTS

Metathesis/Hydrogenation Sequences. Many *trans* bis(phosphine) adducts of rhodium carbonyl chloride have been synthesized by reactions of the dinuclear chloride complex $[(COD)Rh(\mu\text{-}Cl)]_2$, CO, and excess phosphines.[15] As shown in Scheme 2, this procedure was applied to the

Scheme 2. Syntheses and Chloride Ligand Substitution Reactions of Gyroscope-Like Rhodium Complexes

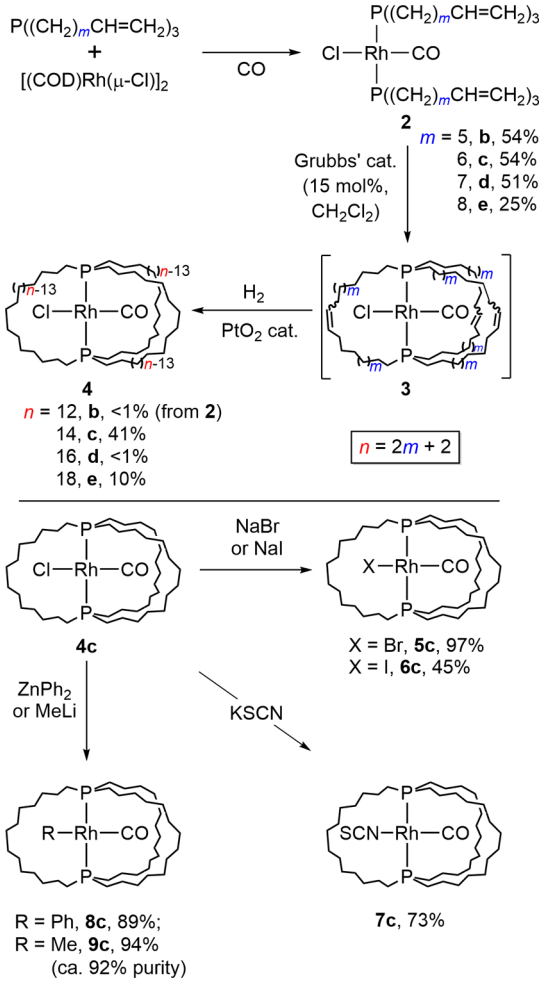

alkene-containing phosphines $P((CH_2)_mCH{=}CH_2)_3$ (m = **b**, 5; **c**, 6; **d**, 7; **e**, 8).[16] Workups gave the target complexes *trans*-$Rh(CO)(Cl)[P((CH_2)_mCH{=}CH_2)_3]_2$ (**2b−e**) as yellow oils in 25−54% yields. These and all other new compounds below were characterized by IR and NMR spectroscopy [^{1}H, ^{13}C{^{1}H}, ^{31}P{^{1}H}], and in most cases microanalyses, as summarized in the Experimental Section. Each complex gave a distinctive IR ν_{CO} band, and NMR spectra exhibited characteristic ^{31}P-derived virtual[17] and ^{103}Rh couplings.

https://doi.org/10.1021/acs.organomet.1c00708
Organometallics 2022, 41, 733−749

Dilute CH_2Cl_2 solutions of **2b−e** (0.0018−0.0020 M) were treated with Grubbs' catalyst (15−22 mol %). Chromatographic workups gave the crude ring-closing metathesis products *trans*-Rh(CO)(Cl)[P((CH$_2$)$_m$CH═CH(CH$_2$)$_m$)$_3$P] (**3b,c,e**) as mixtures of *E*/*Z* C═C isomers. These were partially characterized. The complex with the smallest macrocycle, fifteen-membered **3b**, was only obtained in 3% yield, paralleling findings with related group 10 educts (<1%, ML_y = $PdCl_2$).[7a,18] Presumably mainly oligomers and polymers form. No monorhodium product was detected in the case of **2d**. The phosphine ligand P((CH$_2$)$_7$CH═CH$_2$)$_3$ is also a poor performer in other square planar systems (4%, ML_y = $PtCl_2$).[7a]

The two samples obtained in quantity (**3c,e**) were hydrogenated over PtO_2 (Adams' catalyst) to give the target complexes *trans*-Rh(CO)(Cl)[P((CH$_2$)$_n$)$_3$P] (**4c,e**; $n = 2m + 2$ = **c**, 14; **e**, 18) as yellow powders in 54 and 13% yields, respectively (41% and 10% from **2c,e**). Yields were also lower for the larger ring size in the $PtCl_2$ series. The IR ν_{CO} values of **4c,e**, were similar to those of **2c,e** (1950−1946 vs 1953−1950 cm^{-1}), indicating a negligible cage effect.

Ambient temperature $^{13}C\{^1H\}$ NMR spectra of **4c** in CD_2Cl_2 or $CDCl_3$ showed seven CH_2 signals, or one type of P(CH$_2$)$_{14}$P bridge, as depicted in Figure 1 (bottom). As is commonly seen for such dibridgehead diphosphine adducts, two of the signals exhibited virtual coupling to phosphorus.[17] 2D NMR experiments with $PtCl_2$ analogues have established that the P<u>C</u>H$_2$ signals exhibit the larger couplings (16.2−16.3 Hz), and the PCH$_2$CH$_2$<u>C</u>H$_2$ signals the smaller couplings (6.6−6.8 Hz).[7a] For the square planar rhodium complexes herein, the values range from 11.3 to 13.8 and 6.3 to 7.5 Hz, respectively. Couplings for the PCH$_2$<u>C</u>H$_2$ signals are much smaller, as can be bounded by the widths of the peaks at half-height ($w_{1/2}$ = 2.7−3.4 Hz for **4c,e**). Of relevance to trigonal bipyramidal complexes below, the same trends have been established for Fe(CO)$_3$ analogues,[5a] although the upfield/downfield sense of the P<u>C</u>H$_2$CH$_2$<u>C</u>H$_2$ signals can invert.

Chloride Ligand Substitution Reactions. The chloride ligands in complexes of the type *trans*-Rh(CO)(Cl)(PR$_3$)$_2$ are easily substituted.[19] Could such reactions take place equally well within the cage-like dibridgehead diphosphine ligands of **4c,e**? Accordingly, two types of transformations were pursued. The first involved halide or pseudohalide nucleophiles, and the second involved simple carbon or hydride nucleophiles.

As shown in Scheme 2, CH_2Cl_2 or acetone solutions of **4c** were treated with NaBr, NaI, or KSCN (1.2−10 equiv). Workups gave the corresponding halide or pseudohalide complexes *trans*-Rh(CO)(X)[P((CH$_2$)$_{14}$)$_3$P] (X = **5c**, Br; **6c**, I; **7c**, −NCS) as yellow powders in 45−97% yields. The structures of the first two were confirmed crystallographically as described below. The formulation of **7c** as an isothiocyanate or RhNCS complex was made by analogy to products derived from other *trans*-Rh(CO)(Cl)(PR$_3$)$_2$ species and KSCN and the close correspondence of the IR ν_{NCS} values (2084 vs 2089−2100 cm^{-1}).[20] In contrast to the halide complexes **5c** and **6c**, **7c** exhibited two sets of CH$_2$ $^{13}C\{^1H\}$ signals at room temperature, with one set more intense (ca. 2:1). This is illustrated in Figure 1 (middle), and the dichotomy is rationalized in the Discussion section.

Next, a THF solution of **4c** was treated with $ZnPh_2$ (2.1 equiv), a reagent that effected chloride ligand substitution with the $PtCl_2$ analogue.[7a] A chromatographic workup gave the

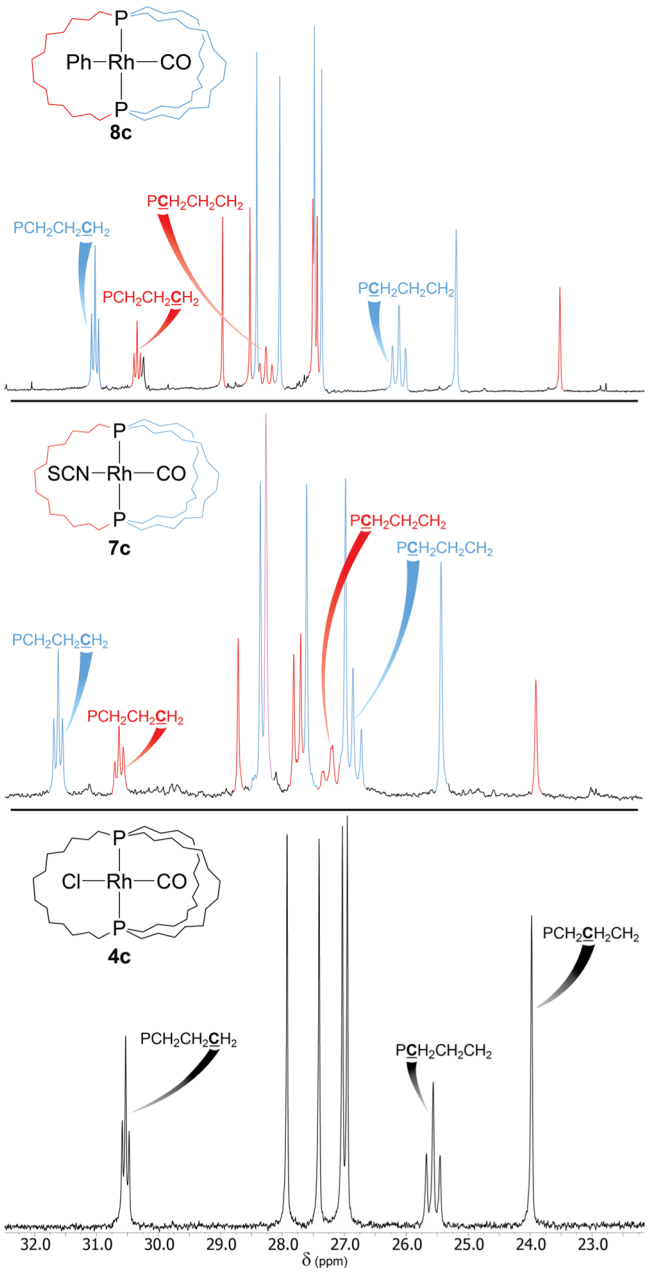

Figure 1. $^{13}C\{^1H\}$ NMR spectra (ambient probe temperature) of the methylene region of **4c** (bottom, $CDCl_3$, 125 MHz), **7c** (middle, toluene-d_8, 100 MHz), and **8c** (top, C_6D_6, 125 MHz).

phenyl complex *trans*-Rh(CO)(Ph)[P((CH$_2$)$_{14}$)$_3$P] (**8c**) in 89% yield. The NMR spectra showed features characteristic of hydrocarbyl bis(phosphine) rhodium complexes, such as strong couplings between rhodium, phosphorus, and the ligating *ipso* and CO carbon atoms ($^1J_{RhP}$ = 142 Hz; $^1J_{RhC(i\text{-}Ph)}$ = 26.4 Hz and $^2J_{PC(i\text{-}Ph)}$ = 16.3 Hz; $^1J_{RhCO}$ = 55.3 Hz and $^2J_{PCO}$ = 13.8 Hz). As with **7c**, the $^{13}C\{^1H\}$ NMR spectrum exhibited two sets of seven CH_2 signals, with a ca. 2:1 area ratio (Figure 1, top).

A similar reaction was conducted with a hexane solution of **4c** and MeLi/LiBr (10 equiv). A number of workups were evaluated, as well as other methyl nucleophiles. In all cases, the target methyl complex *trans*-Rh(CO)(Me)[P((CH$_2$)$_{14}$)$_3$P] (**9c**) was obtained. However, it has not yet been proved

https://doi.org/10.1021/acs.organomet.1c00708
Organometallics 2022, 41, 733−749

possible to isolate **9c** in an analytically pure form. Rather, a material of roughly 92% purity by ^{31}P NMR is obtained in 94% yield (one byproduct). Nonetheless, the methyl ^{1}H and ^{13}C NMR signals were readily apparent as rhodium- and phosphorus-coupled doublets of triplets [^{1}H and ^{13}C{^{1}H} (ppm, C_6D_6): −0.22 (dt, $^{2}J_{RhH}$ = 1.5 Hz, $^{3}J_{PH}$ = 8.3 Hz) and −5.3 (dt, $^{1}J_{RhC}$ = 20.1 Hz, $^{2}J_{PC}$ = 13.9 Hz)]. As with the halide complexes **4c**, **5c**, and **6c**, the ^{13}C{^{1}H} NMR spectrum exhibited a single set of CH_2 signals.

Finally, a THF solution of **4c** was treated with excess $NaBH_4$. As shown in Scheme 3, the workup gave the bidentate

Scheme 3. Reactions Involving Additions to the Rotators of Gyroscope-Like Rhodium Complexes

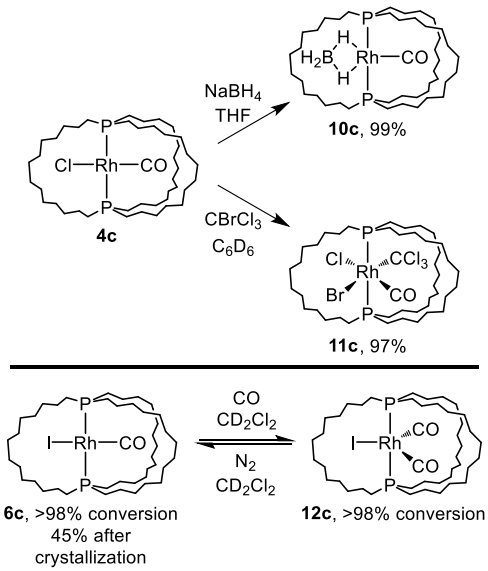

borohydride complex *trans*-Rh(CO)(H$_2$BH$_2$)[P((CH$_2$)$_{14}$)$_3$P] (**10c**) in 99% yield. A number of group 9 halide complexes gave analogous substitution/addition products upon reaction with $NaBH_4$.[21,22] In this case, the structure was evidenced by a broad ^{1}H NMR signal integrating to 4H and anchored by two poorly defined humps (−0.93, −1.05 ppm), in accord with literature precedent.[21] The IR spectrum showed a weak ν_{BH} band at 2394 cm^{-1}. The tetradeutero analogue **10c**-d_4 was analogously synthesized using $NaBD_4$ and exhibited an IR ν_{BD} band at 1697 cm^{-1}. The ν_{BD}/ν_{BH} ratio, 0.709, was in good agreement with that calculated from the reduced masses of the atoms (0.736 for ^{11}B)[23] and reports for other pairs of BH/BD compounds.[22a,24] The ^{13}C{^{1}H} NMR spectra of **10c** and **10c**-d_4 showed a single set of CH_2 signals.

In connection with other objectives, the corresponding hydride complex *trans*-Rh(CO)(H)[P((CH$_2$)$_{14}$)$_3$P] was sought. To the best of our knowledge, there are no examples of BH_3 abstractions from bidentate borohydride complexes to give isolable complexes of the formula Rh(CO)(H)(PR$_3$)$_2$. Nonetheless, **10c** was treated with several nitrogen Lewis bases that are capable of binding BH_3. While no reaction took place with excess pyrazine by ^{31}P{^{1}H} NMR (THF, RT), there was substantial conversion to a new species with excess DMAP or DABCO (toluene, RT), but a rhodium hydride complex could not be detected by ^{1}H or (indirectly) ^{31}P NMR.

Addition Reactions. The preceding reactions with $NaBH_4$ and $NaBD_4$ can be viewed as additions. However, transformations in which the original ligand set of **4c** was retained, with only an increase in coordination number, were also sought. If any of these could be effected reversibly, it could represent a means of modulating the rotational barrier of the rotator.

There is a prior literature of oxidative additions of tetrahalomethanes to square planar d^8 complexes.[25] Accordingly, **4c** and $CBrCl_3$ were combined in C_6D_6. As shown in Scheme 3, the octahedral adduct **11c** was isolated in 97% yield. The stereochemistry (Br and CCl_3 *trans*; Cl and CO *trans*) was tentatively assigned by analogy to that of a crystallographically characterized analogue.[25a] As analyzed below, certain dimensions of the CCl_3 ligand greatly exceeded those of the others in this study. Accordingly, ^{13}C{^{1}H} NMR spectra (room temperature, C_6D_6, or 60 °C, toluene-d_8) exhibited *three* sets of seven CH_2 signals, as depicted in Figure 2. Although not all

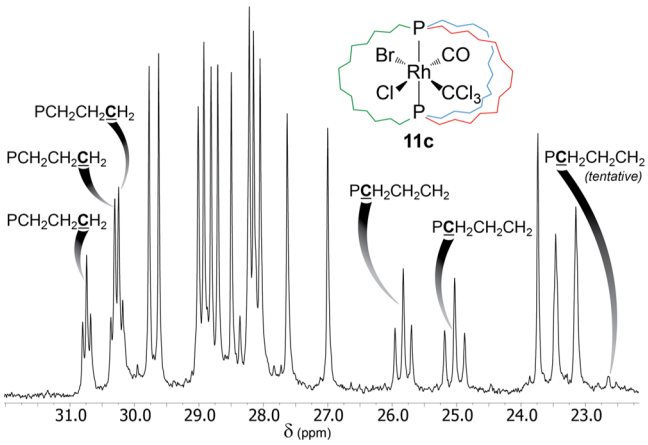

Figure 2. ^{13}C{^{1}H} NMR spectrum of the methylene region of **11c** (C_6D_6, 100 MHz, ambient probe temperature).

peaks are resolved, the three downfield triplets associated with the PCH$_2$CH$_2$C$\underline{H}_2$ signals are easily seen (two partially overlap).[26] As detailed in the Discussion section, this reflects both the higher barrier and lower symmetry associated with the tetrasubstituted rotator.

Next, the reaction of **4c** and NaI was repeated in the presence of CO. Under similar conditions, several trigonal bipyramidal dicarbonyl iodide complexes *trans*-Rh(CO)$_2$(I)(PR$_3$)$_2$ have been generated.[12] These are usually quite labile, reverting to the corresponding monocarbonyl iodide complexes under N_2. As shown in Scheme 3, the dicarbonyl iodide complex **12c** was quantitatively generated. The IR spectrum exhibited two ν_{CO} bands, as opposed to the single absorption for **6c** [1988 (m) and 1930 (s) vs 1940 (s) cm^{-1}]. The ^{31}P{^{1}H} NMR signal was somewhat downfield of that of **6c** (25.2 vs 15.8 ppm, $^{1}J_{PRh}$ 85 vs 113 Hz). Crystals could be grown (CH_2Cl_2/methanol), but sufficed only for a preliminary structure solution that showed the staggered L$_3$M−P(CH$_2$)$_3$ conformation seen for other trigonal bipyramidal adducts of **1c**.[5,6a] When **12c** was purged under a N_2 stream, **6c** was quantitatively regenerated. Low-temperature ^{13}C{^{1}H} NMR spectra of **12c** are described below.

Crystallography. Crystal structures were sought for as many of the preceding complexes as possible. Accordingly, suitable crystals of the bromide, iodide, phenyl, and borohydride complexes **5c**, **6c**, **8c**, and **10c** were obtained, and their structures determined as outlined in Table 1 and the

https://doi.org/10.1021/acs.organomet.1c00708
Organometallics 2022, 41, 733−749

Table 1. Summary of Crystallographic Data

	5c	6c	8c	10c
empirical formula	$C_{43}H_{84}BrOP_2Rh$	$C_{43}H_{84}IOP_2Rh$	$C_{49}H_{89}OP_2Rh$	$C_{43}H_{88}BOP_2Rh$
formula weight	861.86	908.85	859.05	796.79
temperature [K]	110(2)	173(2)	110(2)	110(2)
diffractometer	Bruker D8 GADDS	Nonius KappaCCD	Bruker APEX 2	Bruker D8 GADDS
wavelength [Å]	1.54178	0.71073	0.71073	1.54178
crystal system	monoclinic	monoclinic	monoclinic	monoclinic
space group	$C2/c$	$C2/c$	$P2_1$	$P2_1/c$
unit cell dimensions				
a [Å]	23.2142(12)	23.4154(4)	13.598(2)	20.043(3)
b [Å]	12.2225(6)	12.3194(3)	14.214(2)	15.3822(19)
c [Å]	34.0851(17)	34.0731(8)	13.828(2)	14.884(2)
α [deg]	90	90	90	90
β [deg]	108.563(3)	109.066(1)	113.014(2)	97.445(6)
γ [deg]	90	90	90	90
volume [Å^3]	9168.0(8)	9289.7(4)	2460.0(6)	4550.0(11)
Z	8	8	2	4
ρ_{calcd} [Mg m^{-3}]	1.249	1.300	1.160	1.163
μ [mm^{-1}]	4.894	1.130	0.444	3.897
$F(000)$	3680	3824	932	1736
crystal size [mm^3]	0.07 × 0.06 × 0.05	0.20 × 0.20 × 0.10	0.15 × 0.12 × 0.03	0.06 × 0.03 × 0.02
Θ range [deg]	2.73−60.50	1.26−27.49	1.60−27.50	3.63−59.99
index ranges	$-26 \le h \le 25$	$-30 \le h \le 30$	$-17 \le h \le 17$	$-22 \le h \le 22$
	$-13 \le k \le 13$	$-15 \le k \le 15$	$-18 \le k \le 18$	$-17 \le k \le 17$
	$-38 \le l \le 38$	$-44 \le l \le 44$	$-17 \le l \le 17$	$-16 \le l \le 16$
reflections collected	35769	18326	28440	35375
independent reflections	6853 [R(int) = 0.0524]	10641 [R(int) = 0.0562]	11138 [R(int) = 0.0383]	6630 [R(int) = 0.1262]
max. and min. transmission	0.7919 and 0.7257	0.8954 and 0.8056	0.9868 and 0.9364	0.9261 and 0.7998
data/restraints/parameters	6853/0/433	10641/3/447	11138/106/478	6630/109/433
goodness-of-fit on F^2	1.075	0.947	1.041	1.036
final R indices [$I > 2\sigma(I)$]	R1 = 0.0431, wR2 = 0.1106	R1 = 0.0494, wR2 = 0.1051	R1 = 0.0548, wR2 = 0.1457	R1 = 0.0633, wR2 = 0.1408
R indices (all data)	R1 = 0.0486, wR2 = 0.1128	R1 = 0.1181, wR2 = 0.1433	R1 = 0.0616, wR2 = 0.1522	R1 = 0.1319, wR2 = 0.1583
largest diff. peak and hole [e Å^{-3}]	2.068 and −0.841	0.711 and −0.647	1.440 and −0.579	0.702 and −0.731

Experimental Section. The results are depicted in Figures 3 and 4, and key metrical parameters are given in Table 2. Tables of torsion angles, which can be used to compare the conformations of the dibridgehead diphosphine ligands, are given in the Supporting Information.

The structures of the bromide and borohydride complexes **5c** and **10c** were free of complications. However, the I−Rh−CO moiety in **6c** was disordered, with two orientations differing by ca. 180°. These refined to an 89:11 occupancy ratio, and only the dominant rotamer is shown in Figure 3. As is evident in Figure 3, **5c** and **6c** are essentially isostructural, with P−C−C−C and C−C−C−C torsion angles that always match within a few degrees (Table s1). Also, the space groups are identical ($C2/c$) with very similar unit cell dimensions (Table 1).

Interestingly, the phenyl complex **8c** crystallized in a chiral non-centrosymmetric space group ($P2_1$; no. 33), with only a single enantiomer in the unit cell. The bulk sample was not further investigated, but crystals containing the opposite enantiomer would be anticipated. Although stereogenic atoms are absent, the molecular conformation is chiral. However, such enantiomers would be expected to rapidly interconvert in solution.

Low Temperature $^{13}C\{^1H\}$ NMR Data. When $^{13}C\{^1H\}$ NMR spectra of the square planar chloride or iodide complexes **4c** or **6c** were recorded in $CDFCl_2$ at −120 °C, only severely broadened signals were observed. There were no signs of decoalescence, meaning the fast exchange regime extends to very low temperatures. Similar observations have been made with $PtCl_2$ and $PdCl_2$ analogues.[7a] However, as noted in Figure 1, the NCS and phenyl complexes **7c** and **8c**, each of which features a ligand with a longer radial extension, exhibited two sets of CH_2 ^{13}C signals at room temperature (ca. 2:1 area ratio).

Low temperature $^{13}C\{^1H\}$ NMR spectra of the trigonal bipyramidal dicarbonyl iodide complex **12c** were recorded under CO (1 atm) and showed two sets of CH_2 signals, with one set more intense (ca. 2:1). Hence, the second CO ligand allows the slow exchange regime to be accessed. Upon warming, the sets coalesced, as illustrated for the $PCH_2\underline{C}H_2$ signals in Figure 5 (T_{coal} = 278 K). Cooling regenerated the original spectra. The moderate temperature dependence of the chemical shifts in Figure 5 is typical for gyroscope-like complexes.[5]

Line shape analyses allowed k_{obs} values to be estimated at seven temperatures from 248 to 303 K (Figure 5). An Eyring plot (Figure S1) gave $\Delta H^{\ddagger}$ and $\Delta S^{\ddagger}$ values of 18.6 kcal/mol and 20.3 eu. The nature of the CO signal also varied with temperature. At lower temperatures, a doublet of triplets was observed (−40 °C: $^1J_{RhC}$ = 71.5 Hz, $^2J_{PC}$ = 16.0 Hz). As the coalescence temperature was approached, the couplings became less well resolved. Only a broad singlet was observed at the coalescence temperature or above. The mechanistic

https://doi.org/10.1021/acs.organomet.1c00708
Organometallics 2022, 41, 733−749

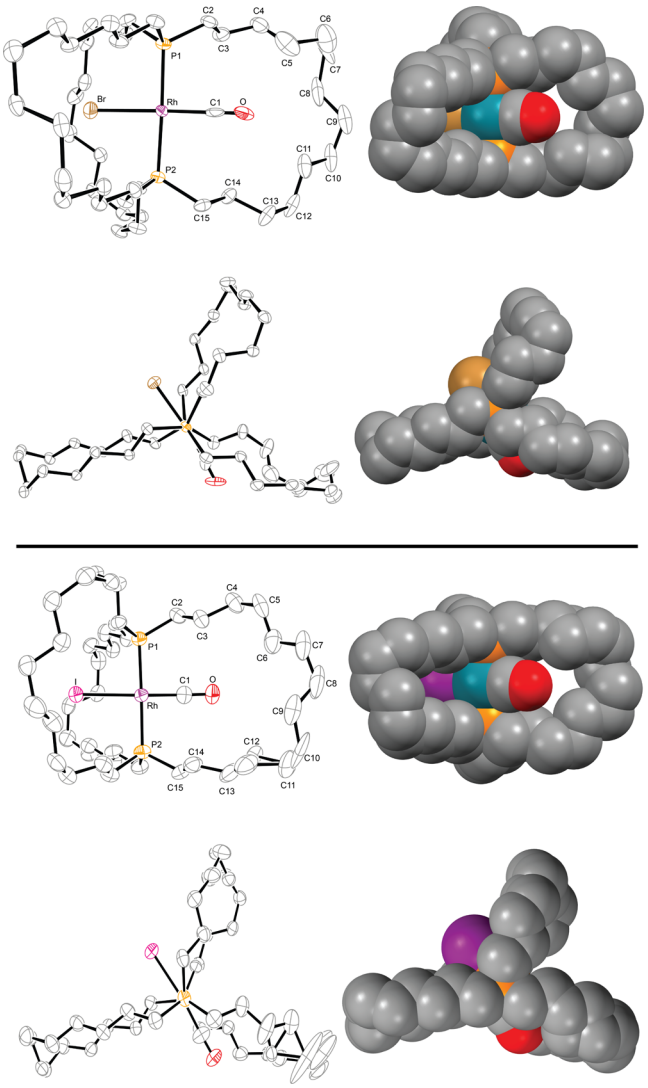

Figure 3. Thermal ellipsoid diagrams (50% probability) and space filling representations of the bromide complex **5c** (top) and iodide complex **6c** (bottom; dominant rotator conformation only).

implications of these data are analyzed in the Discussion section.

Diphosphine Ligand Substitution. The carbonyl and dibridgehead diphosphine ligands of **4c** also present possibilities for substitution chemistry. As noted for the $PtCl_2$ analogue in Scheme 1, reactions with excesses of cyanide and acetylide nucleophiles afford the free diphosphine $P((CH_2)_{14})_3P$ (**1c**).[7a] Salts of the platinum dianion $[Pt(C{\equiv}X)_4]^{2-}$ can also be isolated. Accordingly, we sought to probe the chemistry of **4c** and highly nucleophilic and Lewis basic phosphines.

Thus, as shown in Scheme 4, a hexane solution of **4c** was treated with a toluene solution of PMe_3 (10 equiv). A yellow solid precipitated, and the workup gave the previously characterized bis(phosphine) complex *trans*-Rh(CO)(Cl)-$(PMe_3)_2$ (**13**)[27] in 72% yield. Chromatography of the filtrate afforded **1c** as a colorless solid in 58% yield. Hence, under appropriate conditions, the Rh(CO)(Cl) fragment can, like $PtCl_2$, "escape" from the diphosphine cage.

To probe this process, PMe_3 was added in 1.0 equiv increments to a toluene-d_8 solution of **4c** in an NMR tube.

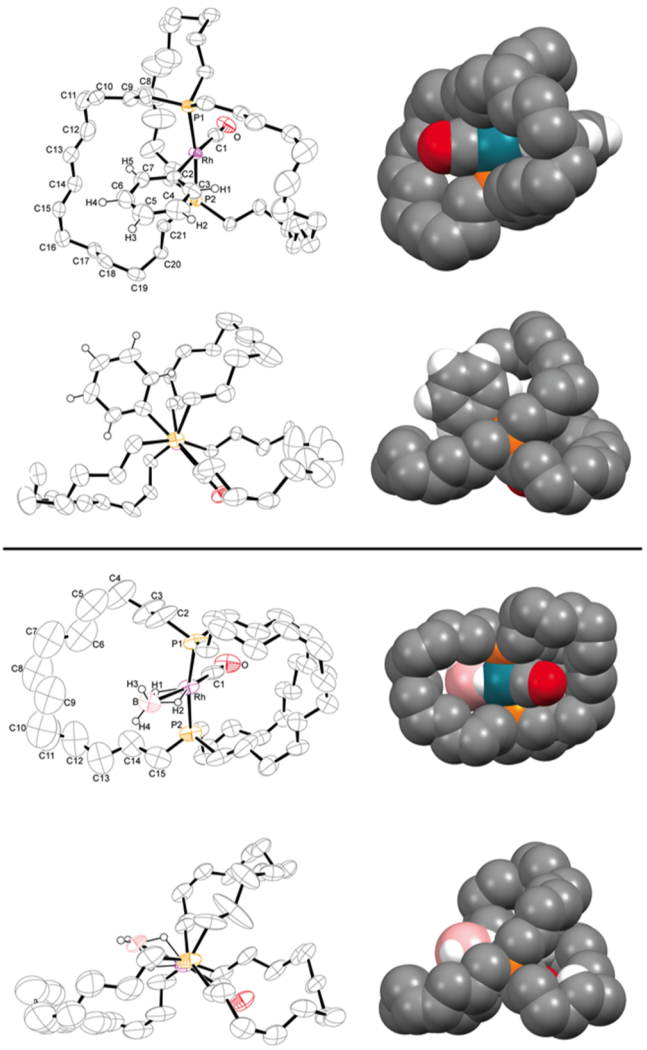

Figure 4. Thermal ellipsoid diagrams (50% probability) and space filling representations of the phenyl complex **8c** (top) and μ^2-borohydride complex **10c** (bottom).

Table 2. Key Crystallographic Distances [Å] and Angles [deg]

	5c	6c	8c	10c
Rh−P1	2.320(1)	2.3247(14)	2.309(1)	2.320(2)
Rh−P2	2.323(1)	2.3220(14)	2.304(2)	2.323(2)
Rh−CO	1.858(6)	1.775(7)	1.878(5)	1.806(8)
C−O	1.015(7)	1.176(8)	1.101(6)	1.15(1)
Rh−X[a]	2.5056(6)	2.6801(5)	2.137(5)	2.326(8)
Rh−H				1.5397
				1.5202
P1−Rh−P2	177.81(4)	178.38(5)	177.81(4)	169.34(8)
P1−Rh−C	92.4(2)	89.5(2)	92.4(2)	89.3(3)
P2−Rh−C	89.7(2)	91.9(2)	93.7(2)	88.5(3)
P1−Rh−X[a]	86.67(3)	91.75(4)	86.7(2)	90.1(2)
P2−Rh−X[a]	91.24(3)	86.97(4)	87.6(2)	93.7(2)
C−Rh−X[a]	174.3(2)	173.4(2)	176.0(2)	171.2(3)
Rh−C−O	177.5(5)	177.3(7)	178.2(5)	179.3(7)

[a]X = Br, I, C_{ipso}, or B.

Within 20 min of the addition of the first equiv, some **13** could be detected by $^{31}P\{^1H\}$ NMR.[28] After 5.0 equiv, the signals of **4c** had nearly disappeared. After 4.0 equiv, broad low intensity

https://doi.org/10.1021/acs.organomet.1c00708
Organometallics 2022, 41, 733−749

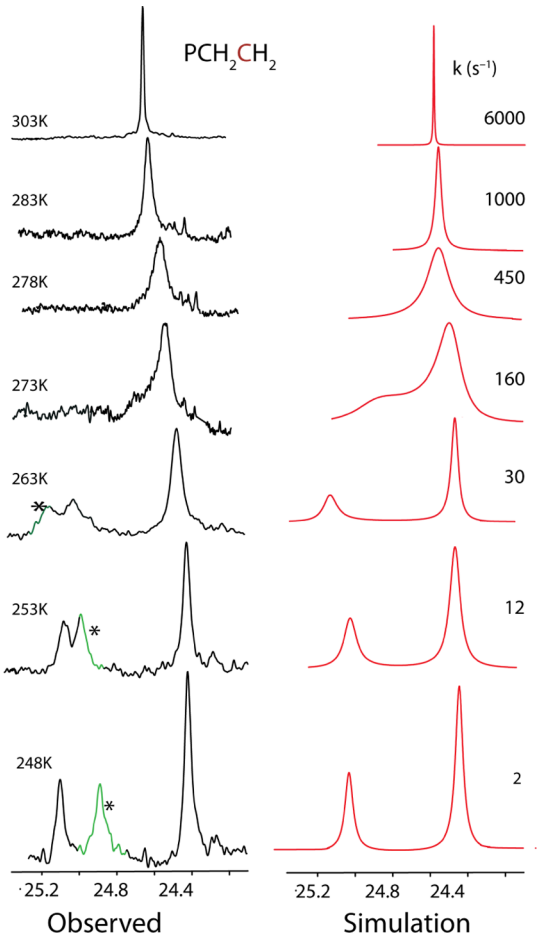

Figure 5. Variable temperature $^{13}C\{^1H\}$ NMR spectra of **12c** (CD_2Cl_2, 100 MHz) under CO (1 atm; the signal designated with a * is from another CH_2 group).

Scheme 4. Displacement/Reinsertion of the Rh(CO)(Cl) Rotator From/Into the Dibridgehead Diphosphine 1c

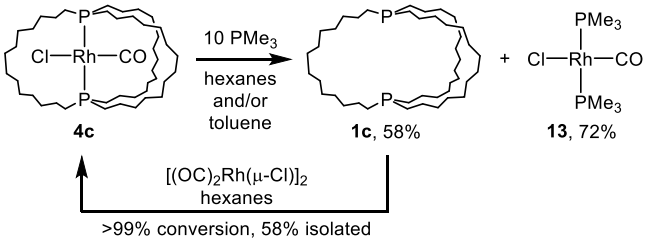

peaks due to **1c** and PMe_3 could be discerned. These sharpened and intensified after 6.0 equiv of PMe_3 had been added. Several minor signals, coupled to both rhodium and phosphorus, were apparent. Possible intermediates are proposed in the Discussion section. However, no significant quantities of the tris(phosphine) complex $Rh(Cl)(PMe_3)_3$, which exhibits distinctive ^{31}P NMR signals,[29] were detected.

The reversibility of the displacement of the rhodium rotator from **4c** was tested. As shown in Scheme 4, a hexane solution of $[(OC)_2Rh(\mu\text{-}Cl)]_2$ was treated with **1c**. Analysis of an aliquot by ^1H and $^{31}P\{^1H\}$ NMR showed >99% conversion to **4c**, which was subsequently isolated in 58% yield.

DISCUSSION

Syntheses. Schemes 2−4 show that a variety of gyroscope-like rhodium complexes containing aliphatic *trans* dibridgehead diphosphine ligands $P((CH_2)_n)_3P$ can be accessed by three-fold intramolecular ring-closing metatheses and subsequent hydrogenation, substitution, and/or addition reactions. The metathesis/hydrogenation sequences are most effective for n = 14, and thus, the chemistry of **4c** has been most extensively developed. In general, it appears possible to reproduce virtually all standard rhodium(I) chemistry within the diphosphine cage. These transformations also allow direct access to species with sterically shielded dipolar rotators, in contrast to routes involving PtX_2 or similar analogues, for which monosubstitution to give Pt(X)(Y) adducts is normally problematic.[7a,9]

Rotator Dimensions. In order to rationalize the broad range of dynamic properties exhibited by the rhodium complexes, several concepts must be introduced. First, every rotator ML_y is characterized by a "van der Waals radius". This would be determined by the ligand with the greatest individual radius. For many ligands, one can simply take the distance from the metal to the terminal atom, and add the van der Waals radius[30] of the terminal atom. The radii of ligands relevant to this study have been calculated using distances in the crystal structures in Figures 3 and 4 (Table 2), or those of closely related rhodium complexes, and are summarized in Table 3.

For example, in the case of a CO ligand, the rhodium−oxygen distance is added to the van der Waals radius of an oxygen atom, giving 4.46 Å (2.94 + 1.52 Å). In the case of phenyl, the distance from rhodium to the *p*-hydrogen atom is used, giving 7.08 Å (5.88 + 1.20 Å). With the methyl ligand, the van der Waals surfaces of the hydrogen atoms do not extend further from the P−Rh−P axis than that of the carbon atom (the axis is the optimum reference when all atoms do not lie in the trigonal plane). The same holds for the terminal and bridging hydrogen atoms of the μ^2-BH_4 ligand. With the CCl_3 ligand, the van der Waals surfaces of the chlorine atoms *do* extend further from the P−Rh−P axis than that of the carbon atom, but the radius thus obtained remains less than that associated with the iodide ligand (4.59 Å vs 4.66 Å).

Rotators are also capable of steric interactions in an orthogonal or "vertical" dimension, in which "thickness" would play a role. With a halide ligand, this equates to the van der Waals *diameter*. With linear CO or NCS ligands or planar phenyl ligands, this would be derived from the atom with the greatest van der Waals diameter (CO, 3.40 Å for carbon; NCS, 3.60 Å for sulfur). For a methyl ligand, this can be calculated from a static structure (see **A** in Table 3) or the cone defined by rotating the methyl group. The latter is somewhat greater (3.57 Å vs 4.03 Å). Importantly, the "thickness" of the CCl_3 ligand (5.98 Å or 6.80 Å) greatly exceeds the others.

Diphosphine Cage Void Space. The next step in rationalizing dynamic properties involves the void space within the diphosphine cage, a feel for which can be gleamed from the space filling representations in Figures 3 and 4. Figure 6 (left) focuses on the "horizontal clearance" or void space in the plane of the rotator. In an idealized scenario, one would take the distance from rhodium to the distal carbon atoms of the $(CH_2)_{14}$ segments and subtract the van der Waals radius of carbon. In actuality, the three $(CH_2)_{14}$ segments can adopt a number of conformations, as evidenced in Figures 3 and 4 and

https://doi.org/10.1021/acs.organomet.1c00708
Organometallics 2022, 41, 733−749

Table 3. Dimensions Associated with Rotator Ligands L (Å; vdW = van der Waals)

Ligand L	Reference complex[a]	Rh-L vdW radius[b]	L vdW "thickness"[c]
CO	**5c**, **6c**, **8c**, **10c**	4.46[b]	3.40
Cl	Ref 27	4.10	3.50
Br	**5c**	4.36	3.66
I	**6c**	4.66	3.96
NCS	Ref 20c	6.63	3.60
C_6H_5	**8c**	7.08[d]	3.40
CH_3	Ref 27	3.83[e]	3.57 (4.03)[f]
η^2-BH_4	**10c**	4.28[e]	3.84
CCl_3	Ref 19a	4.59[g]	5.98 (6.80)[h]

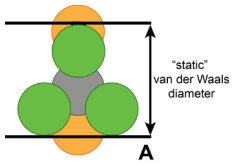

[a]Rhodium complexes used for the distances in *b* and related parameters (averages were taken when multiple complexes are listed). [b]The distance from rhodium or the P−Rh−P axis to the terminal atom of the ligand, *plus* the vdW radius[30] of the terminal atom. [c]Unless footnoted otherwise, this is expressed by the atom with the largest vdW diameter. [d]This value includes the vdW surface of the *p*-hydrogen atom. [e]The vdW surfaces of the CH_3 and terminal BH_2 hydrogen atoms do not extend farther from the P−Rh−P axis than those of the boron and carbon atoms. [f]These values were determined analogously to those for the CCl_3 ligand, as described in *h*. [g]The distance from the P−Rh−P axis to the most remote vdW surface of each chlorine atom (average of three values). [h]The smaller value represents the distance expressed by the double headed arrow in the static structure **A**; the larger represents the vdW diameter swept by rotation of the Rh−CCl_3 bond.

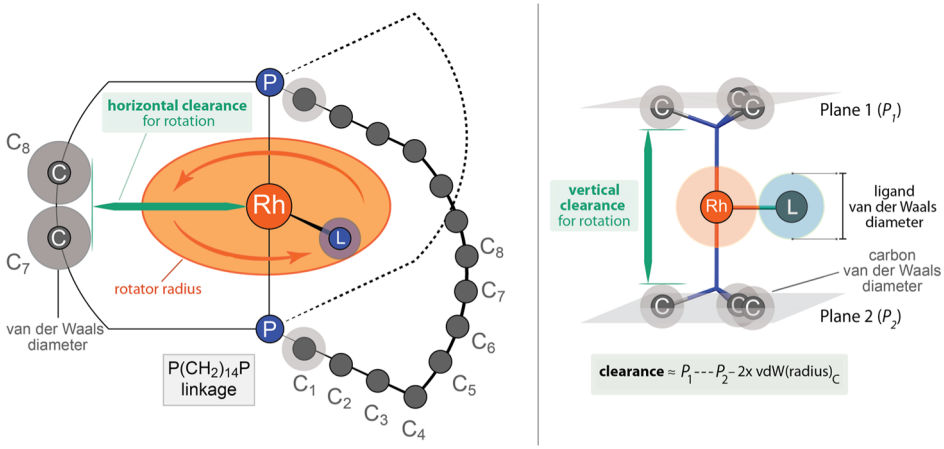

Figure 6. Analyses of the void space in complexes of the dibridgehead diphosphine $P((CH_2)_{14})_3P$ (**1c**).

many other crystal structures.[5,6,7a] Analyses can be carried out using "average clearances" or "minimum clearances" or other treatments. Values of 5−6 Å have been used for various complexes of **1c** in the past,[5,6,7a] and all of the new rhodium complexes fall within these limits.

Figure 6 (right) presents one of several approaches to estimating the "vertical clearance" or void space needed to accommodate the "thickness" or the rotator. First, the distance between the two planes defined by the three CH_2 groups on each phosphorus atom is calculated, and then twice the van der Waals radius of a carbon atom is subtracted.[5a] This gives a rather modest clearance of ca. 2.60 Å, smaller than the van der Waals diameters or "thicknesses" of all the ligands in Table 3. As analyzed extensively elsewhere,[1b,5a,31] ML_y rotation must therefore be correlated to conformational changes in the diphosphine ligands. Accordingly, rotational barriers drop significantly in analogous dibridgehead diarsine complexes, where the metal-heteroatom bonds are ca. 4% longer.[31] However, any ligand with a "thickness" greater than the P−Rh−P distance (ca. 4.60 Å) would be certain to block rotation, even with much longer $(CH_2)_n$ segments.

The key conclusions from this section are (a) both phenyl and NCS ligands markedly exceed the horizontal clearance afforded by dibridgehead diphosphine ligands with $(CH_2)_{14}$ chains; (b) the remaining ligands are accommodated by these clearances; (c) all of the ligands have "diameters" or "thicknesses" that exceed the vertical clearance, but for the CCl_3 ligand, this value is greater than the P−Rh−P distance (≥5.98 Å vs 4.60 Å).

Dynamic Properties, Square Planar Complexes. Consider the reaction coordinate as the Rh(CO)(X) moieties of the square planar rhodium complexes are rotated a full 360°. As illustrated in Figure 7, these constitute six-fold rotational barriers, as six minima (**II**−**VII**) and six intervening maxima (not depicted) are encountered.[32] Note that there are two different rate constants, k_1 and k_2, corresponding to either the Y (CO) or X ligands passing through a macrocycle.

For none of the minima in Figure 7 are any of the three $(CH_2)_n$ bridges equivalent (exchanged by a symmetry operation). Thus, three sets of ^{13}C NMR signals would be expected. Most of the above rhodium complexes give only one, even at the lowest NMR temperatures attainable (X = Cl, Br, I, CH_3, η^2-BH_4). Parallel results have been obtained for the corresponding platinum dihalide complexes (when X = Y in **II**−**VII**, two of the $(CH_2)_{14}$ bridges become equivalent).[7a] This requires rapid $(CH_2)_{14}$ bridge exchange on the NMR time scale, or a 360° rotation in Figure 7.

When the preceding set of ligands is replaced by one with a radius that precludes passage through a $(CH_2)_{14}$ bridge, dynamic behavior becomes restricted. Specifically, this results in a marked decrease in the rate constants, where X must pass through a macrocycle (k_2). However, the rate constants for the

https://doi.org/10.1021/acs.organomet.1c00708
Organometallics 2022, 41, 733−749

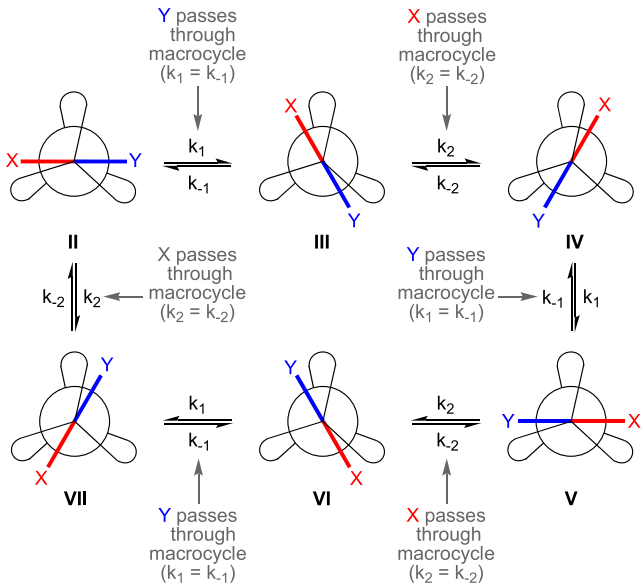

Figure 7. Energy minima associated with the six-fold rotational barriers of square planar X−M−Y (X−Rh−CO) complexes of the dibridgehead diphosphines $P((CH_2)_n)_3P$ (**1**).

steps that involve Y (CO) passing through a macrocycle (k_1) would be less affected. Thus, as illustrated by **VIII** and **IX** in Figure 8 (top), the CO ligand is able to pass between two

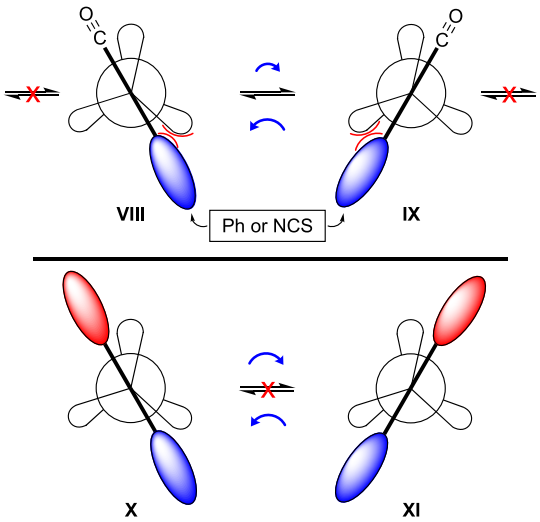

Figure 8. Restrictions on equilibria of the type in Figure 7 when one (top) or both (bottom) of the X−Rh−Y ligands is too large to pass through the diphosphine macrocycle.

adjacent interstices, while the larger ligand (e.g., NCS or phenyl) remains confined to one. This serves to exchange the positions of two $(CH_2)_{14}$ bridges but not the third, resulting in two sets of CH_2 ^{13}C NMR signals as illustrated in Figure 1 (middle, top).

For the sake of completeness, the situation in which X and Y are two large ligands is also diagrammed in Figure 8. Neither can pass through a macrocycle, so three sets of signals would be anticipated at all temperatures. Although the corresponding $PtPh_2$ and $Pt(NCS)_2$ complexes have different symmetries, both are also in the slow exchange limit at ambient temperature (two sets of signals consistent with the mirror plane when the colors are eliminated in **X** and **XI**).[7a] When the bridges are lengthened to $(CH_2)_{16}$, the $PtPh_2$ complex exhibits a single set of signals (fast exchange limit).[7a,33]

Dynamic Properties, Other Coordination Geometries. Next, consider the trigonal bipyramidal dicarbonyl complex **12c** generated in Scheme 3. As shown in Figure 9, such

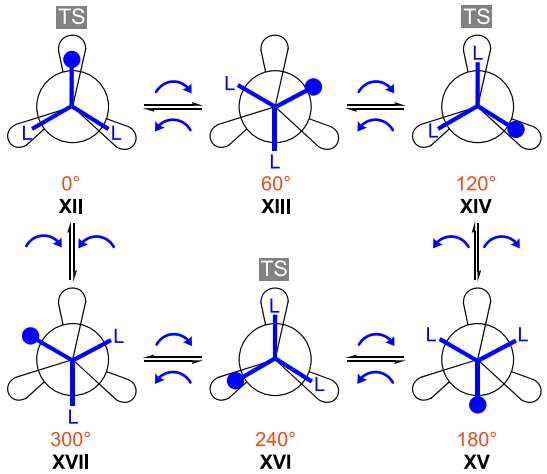

Figure 9. Energy minima and maxima associated with the three-fold rotational barriers of trigonal bipyramidal complexes of the dibridgehead diphosphines $P((CH_2)_n)_3P$ (**1**). The blue dot can be considered a marker or the iodide ligand of a $Rh(CO)_2I$ rotator.

adducts have three-fold rotational barriers,[32] with three maxima and three minima as the rotator passes through 360°. In any minimum of a $Rh(CO)_2(I)$ or similar rotator, two of the $(CH_2)_n$ bridges are symmetry equivalent (e.g., the lower two in **XV**). Note that each transition state exhibits three eclipsing interactions, as opposed to one in Figure 7. Accordingly, there is a general expectation (also from other considerations) that for related compounds, six-fold barriers will be associated with lower activation energies than three-fold barriers.[32]

Low temperature $^{13}C\{^1H\}$ NMR spectra of **12c** clearly show that the slow exchange limit can be reached, unlike the square planar precursor **6c**. Two sets of CH_2 signals are observed, as excerpted in Figure 5. This strongly suggests a much higher rotational barrier than **6c**. However, the mechanism by which the $(CH_2)_{14}$ bridges exchange in the high temperature limit merits scrutiny. In particular, the markedly positive $\Delta S^{\ddagger}$ value (20.3 eu) best fits a dissociative mechanism, which considering the facile equilibrium **6c** + CO ⇄ **12c** would logically involve CO. In contrast, the $\Delta S^{\ddagger}$ value for $Fe(CO)_2(NO)^+$ rotation within the same diphosphine cage is negative (−6.5 eu).[5a] Here, any CO dissociation is excluded by the phosphorus coupling ($^1J_{CP}$) that remains in the fast exchange limit. However, the couplings that can be observed for the CO signal of **12c** in the slow exchange limit (−40 °C: $^1J_{RhC}$ = 71.5 Hz, $^2J_{PC}$ = 16.0 Hz) wash out in the fast exchange limit.

Thus, we conclude that the $(CH_2)_{14}$ bridges in **12c** preferentially exchange by a mechanism involving rate-limiting CO dissociation to give **6c**, followed by rapid Rh(CO)(I) rotation and CO addition, as sketched in Figure 10. An alternative mechanism involving $Rh(CO)_2(I)$ rotation is probably viable but requires a higher activation energy. In any case, these data can be taken as strong support for intrinsically higher three-fold as opposed to six-fold rotational

https://doi.org/10.1021/acs.organomet.1c00708
Organometallics 2022, 41, 733−749

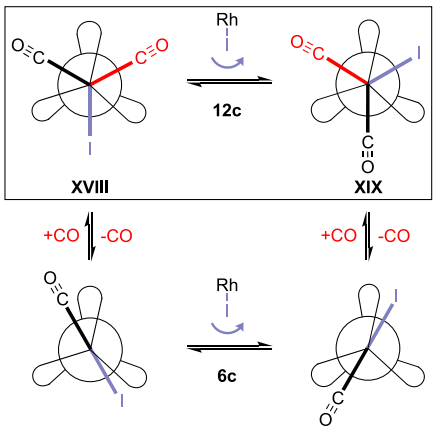

Figure 10. Dissociative (bottom) and non-dissociative (boxed) mechanisms for interconverting rotamers of **12c**.

barriers in these systems.[32] Furthermore, given the facility with which the second CO ligand can bind or dissociate, it can be considered a reversible "brake" or modulator of the rotational barrier.

Octahedral complexes such as **11c** would have twelve-fold rotational barriers, and representative maxima and minima are given in Figure 11 (**XX**−**XXII**). However, since **11c** does not

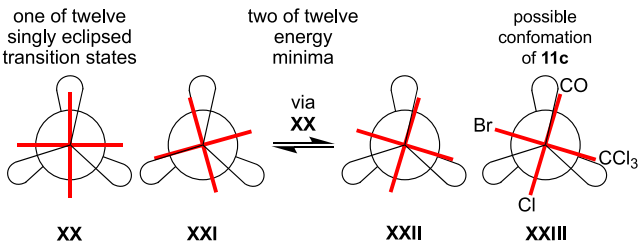

Figure 11. Representative energy minima and maxima associated with the twelve-fold rotational barriers of octahedral complexes of the dibridgehead diphosphines $P((CH_2)_n)_3P$ (**1**).

exhibit dynamic behavior, readers are referred elsewhere for more detailed treatments.[1b,6,31] When the radii of the four equatorial ligands are small, as in certain osmium and rhenium complexes (L = CO, Cl, Br, CH_3, etc.), only the fast exchange limit can be observed, even at very low temperatures.[6] Hence, the CCl_3 ligand in **11c** is solely responsible for blocking rotation.

Note that as shown in **XXI** and **XXII**, one of the three interstices must accommodate two of the four equatorial ligands. This poses the possibility of an unusual type of isomerism that might be detectable in appropriately substituted systems with high rotational barriers. Namely, which two of the four ligands occupy the same interstice? In the crystallographically characterized complex that was used to assign the stereochemistry to **11c**, *trans*-Rh(CO)(Cl)(Br)(CCl_3)-$(PMe_3)_2$,[27] all *trans* P−CH_3 bonds are eclipsed, creating a steric environment related to those in **XXI** and **XXII**. Surprisingly, the doubly occupied interstice does not feature two of the smaller ligands, but rather the large CCl_3 ligand and a CO ligand, as depicted in **XXIII**. However, the CO ligand comes close to being eclipsed with the two proximal P−CH_3 bonds.

Diphosphine Decomplexation and Other Chemistry. Other aspects of the new chemistry herein deserve emphasis. First, the liberation of the dibridgehead diphosphine **1c** from **4c** in Scheme 4 adds to the growing number of reactions in which the rotator ML_y can be excised from the ligand cage.[7a,10] Although much mechanistic work remains to be done, certain evidence points toward the operation of "homeomorphic" isomerizations,[10,34,35] in which the diphosphines literally turn themselves inside out. One such pathway would involve the hypothetical species **14c** in Scheme 5, for which cleavage of a

Scheme 5. Equilibrium that Involves a Homeomorphic Isomerization and May Play a Role in the Chemistry of 4c (Top) and Other Relevant Complexes (Bottom)

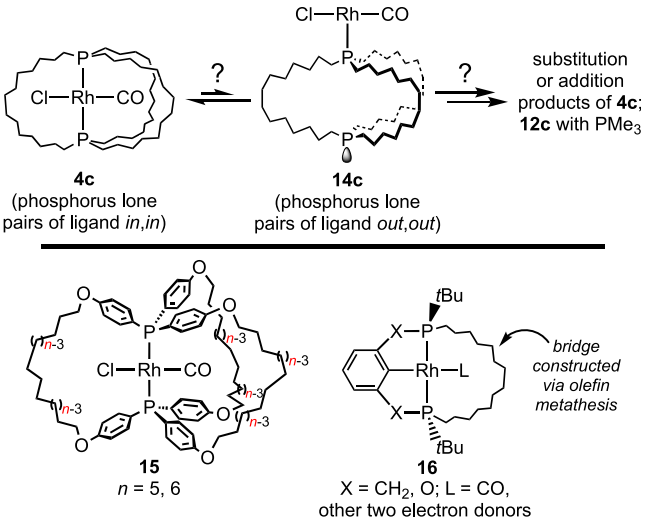

rhodium-phosphorus bond is also necessary. In **4c**, the phosphorus lone pairs of the ligand are both directed "*in*", and in **14c**, they are both "*out*", in what would be termed an *out, out* isomer.[35b]

There would be several possibilities for how **14c** and PMe_3 might then react to give **1c** and **13** (Scheme 4). Furthermore, **14c** could be an intermediate in the chloride ligand substitutions and CO and $CBrCl_3$ additions. Recent computational data indicate that the *in,in* isomer of **1c** is more stable than the *out,out*.[36] Thus, an initial isomerization to *out,out*-**1c** may be required to reinstall the Rh(CO)(Cl) rotator with $[(OC)_2Rh(\mu\text{-}Cl)]_2$ (Scheme 4).

Earlier, we established that certain complexes in this report can serve as catalyst precursors for olefin hydroformylation.[14b] There was potential for the cage-like environment to lead to new selectivities. However, since there are pathways for the rhodium rotators to escape from the cage, or possibly react in altered steric environments such as **14c**, catalysis has not been further pursued. In this context, we have developed another series of gyroscope-like rhodium complexes based upon triarylphosphines, as exemplified by **15** (Scheme 5). These are of interest from a variety of standpoints, but given the "rigid" *p*-phenylene units in the bridges, they may have a higher barrier to homeomorphic isomerization (which entails much torsional motion). Such less flexible systems may help to ensure catalysis within an architecturally defined space.

Finally, there is notable recent work involving other sterically constrained rhodium(I) environments.[37−39] The most relevant features a series of complexes with phosphine pincer ligands that are connected by an additional $(CH_2)_{14}$ bridge, as reported by Chaplin and exemplified by **16** in Scheme 5.[38] Ligands that occupy the cavity can show unique

https://doi.org/10.1021/acs.organomet.1c00708
Organometallics 2022, 41, 733−749

reactivity compared to unbridged analogues, providing further motivation for the continued development of the complexes in Schemes 2−4.

■ CONCLUSION

This study has established the ready availability of a large class of rhodium complexes with sterically shielded dipolar rotators, which can in principle be directed by electric fields. These can be statically applied, creating an analogy of a compass,[40] or dynamically applied, with an appropriate rotational frequency yielding a molecular gyroscope.[1] The dynamic properties of the rotators have been studied in detail, and well-defined trends have emerged based upon the radii and "thicknesses" or "diameters" of the constituent ligands L_y. Additional trends can be defined based upon coordination geometries. This work represents the most comprehensive treatment to date of the factors that control rotational barriers for rotators embedded in cage-like assemblies of the formula $E((CH_2)_n)_3E$, classes of molecules that are continuing to see rapid growth.

■ EXPERIMENTAL SECTION

General. Reactions were conducted under N_2 atmospheres. Solvents and reagents were treated as described in the Supporting Information. The $CDFCl_2$ was prepared by a literature procedure.[41] NMR spectra were obtained on standard FT spectrometers and referenced as follows (δ/ppm): ^{1}H, residual internal $CHCl_3$ (7.26), C_6D_5H (7.16), $CHDCl_2$ (5.32), $CHFCl_2$ (7.47), or $C_6D_5CHD_2$ (2.08); ^{13}C, internal $CDCl_3$ (77.16), C_6D_6 (128.06), CD_2Cl_2 (53.84), $CDFCl_2$ (104.2), or $C_6D_5\underline{C}D_3$ (20.43); ^{31}P{^{1}H}, external H_3PO_4 (0.00). DSC and TGA data were obtained with a Mettler-Toledo DSC-821 instrument and treated by standard methods.[42]

***trans*-Rh(CO)(Cl)[P((CH$_2$)$_5$CH═CH$_2$)$_3$]$_2$ (2b).** A Schlenk flask was charged with [(COD)Rh(μ-Cl)]$_2$ (0.531 g, 1.07 mmol) and CH_2Cl_2 (20 mL), and CO was gently bubbled through the solution. After 15 min, a solution of P[(CH$_2$)$_5$CH═CH$_2$]$_3$ (1.468 g, 4.555 mmol)[16] in hexanes (20 mL) was added. The dark red solution was stirred (16 h). Rotary evaporation gave a dark red oil that was chromatographed on silica (5.0 × 30 cm column) with hexanes (500 mL) followed by hexanes/CH_2Cl_2 (2:1 v/v). The solvent was removed from the product-containing fractions by rotary evaporation to give **2b** as a yellow oil (0.931 g, 1.15 mmol, 54%). Anal. Calcd For $C_{43}H_{78}ClOP_2Rh$: C, 63.65; H, 9.69. Found: C, 63.82; H, 9.64. IR (cm^{-1}, oil film): 1948 (s, ν_{CO}), 1639 (m, $\nu_{C=C}$).

NMR ($CDCl_3$, δ/ppm): ^{1}H (500 MHz) 5.71−5.63 (m, 6H, C**H**═), 4.89−4.78 (m, 12H, ═C**H$_2$**), 1.96−1.89 (m, 12H, C**H$_2$**CH═), 1.75−1.68 (m, 12H, C**H$_2$**), 1.48−1.38 (m, 12H, C**H$_2$**), 1.33−1.25 (m, 24H, C**H$_2$**); ^{13}C{^{1}H} (125 MHz) 188.1 (dt, $^1J_{RhC}$ = 75.4 Hz, $^2J_{PC}$ = 15.7 Hz, **C**O), 138.8 (s, **C**H═), 114.4 (s, ═**C**H$_2$), 33.7 (s, **C**H$_2$), 30.8 (virtual t,[17] $^3J_{PC}$ = 6.3 Hz, PCH$_2$CH$_2$**C**H$_2$), 28.5 (s, **C**H$_2$), 24.46 (virtual t,[17] $^1J_{PC}$ = 12.6 Hz, P**C**H$_2$), 24.39 (s, **C**H$_2$); ^{31}P{^{1}H} (202 MHz) 16.7 (d, $^1J_{RhP}$ = 117 Hz).

***trans*-Rh(CO)(Cl)[P((CH$_2$)$_6$CH═CH$_2$)$_3$]$_2$ (2c).** A Schlenk flask was charged with P[(CH$_2$)$_6$CH═CH$_2$]$_3$ (1.495 g, 4.10 mmol),[16] CH_2Cl_2 (20 mL), hexane (20 mL), and [(COD)Rh(μ-Cl)]$_2$ (0.493 g, 1.00 mmol) and flushed with CO. The orange solution was stirred and turned deep yellow. After 2 h, the solvent was removed by oil pump vacuum. The tan oil was chromatographed on silica gel (2.5 × 7.0 cm column) with hexane/CH_2Cl_2 (2:1 v/v). The solvent was removed from the product-containing fractions by oil pump vacuum to give **2c** as a yellow oil (1.306 g, 1.458 mmol, 73%). Anal. Calcd for $C_{49}H_{90}ClOP_2Rh$: C, 65.72; H, 10.13; Found: C, 65.28; H, 9.70. IR (cm^{-1}, powder film): 1953 (s, ν_{CO}).

NMR ($CDCl_3$, δ/ppm): ^{1}H (400 MHz) 5.93−5.71 (m, 6H, C**H**═), 4.98−4.96 (m, 12H, ═C**H$_2$**), 2.00 (q, $^3J_{HH}$ = 6.8 Hz, 12H, C**H$_2$**CH═), 1.80−1.70 (m, 12H, C**H$_2$**), 1.52−1.49 (m, 12H, C**H$_2$**), 1.40−1.25 (m, 36H, C**H$_2$**); ^{13}C{^{1}H} (100 MHz) 187.9 (dt, $^1J_{RhC}$ = 75.6 Hz, $^2J_{PC}$ = 15.7 Hz, **C**O), 138.7 (s, **C**H═), 114.1 (s, ═**C**H$_2$), 33.5 (s, **C**H$_2$), 32.0 (virtual t,[17] $^3J_{PC}$ = 6.5 Hz, PCH$_2$CH$_2$**C**H$_2$), 28.6 (s, **C**H$_2$), 28.5 (s, **C**H$_2$), 24.6 (virtual t,[17] $^1J_{PC}$ = 12.8 Hz, P**C**H$_2$), 24.4 (s, **C**H$_2$); ^{31}P{^{1}H} (162 MHz) 17.6 (d, $^1J_{RhP}$ = 115 Hz).

***trans*-Rh(CO)(Cl)[P((CH$_2$)$_7$CH═CH$_2$)$_3$]$_2$ (2d).** [(COD)Rh(μ-Cl)]$_2$ (0.778 g, 1.58 mmol), CH_2Cl_2 (20 mL), CO, and a solution of P[(CH$_2$)$_7$CH═CH$_2$]$_3$ (2.626 g, 6.462 mmol)[16] in hexanes (20 mL) were combined in a procedure analogous to that for **2b**. An identical workup gave **2d** as a yellow oil (1.574 g, 1.608 mmol, 51%). Anal. Calcd For $C_{55}H_{102}ClOP_2Rh$: C, 67.43; H, 10.49. Found: C, 67.16; H, 10.61. IR (cm^{-1}, oil film): 1950 (s, ν_{CO}), 1639 (m, $\nu_{C=C}$).

NMR ($CDCl_3$, δ/ppm): ^{1}H (500 MHz) 5.83−5.75 (m, 6H, C**H**═), 5.00−4.90 (m, 12H, ═C**H$_2$**), 2.05−2.00 (m, 12H, C**H$_2$**CH═), 1.86−1.80 (m, 12H, C**H$_2$**), 1.57−1.50 (m, 12H, C**H$_2$**), 1.42−1.25 (m, 48H, C**H$_2$**); ^{13}C{^{1}H} (125 MHz) 188.2 (dt, $^1J_{RhC}$ = 76.7 Hz, $^2J_{PC}$ = 15.7 Hz, **C**O), 139.2 (s, **C**H═), 114.3 (s, ═**C**H$_2$), 33.9 (s, **C**H$_2$), 31.4 (virtual t,[17] $^3J_{PC}$ = 6.3 Hz, PCH$_2$CH$_2$**C**H$_2$), 29.2 (s, **C**H$_2$), 29.1 (s, **C**H$_2$), 29.0 (s, **C**H$_2$), 24.6 (s, **C**H$_2$), 24.5 (virtual t,[17] $^1J_{PC}$ = 12.6 Hz, P**C**H$_2$); ^{31}P{^{1}H} (202 MHz) 16.6 (d, $^1J_{RhP}$ = 115 Hz).

***trans*-Rh(CO)(Cl)[P((CH$_2$)$_8$CH═CH$_2$)$_3$]$_2$ (2e).** [(COD)Rh(μ-Cl)]$_2$ (0.812 g, 1.65 mmol), CH_2Cl_2 (20 mL), CO, and a solution of P[(CH$_2$)$_8$CH═CH$_2$]$_3$ (3.031 g, 6.754 mmol)[16] in hexanes (20 mL) were combined in a procedure analogous to that for **2b**. An identical workup gave **2e** as a yellow oil (0.891 g, 0.837 mmol, 25%). Anal. Calcd For $C_{61}H_{114}ClOP_2Rh$: C, 68.87; H, 10.80. Found: C, 68.58; H, 11.04. IR (cm^{-1}, oil film): 1950 (s, ν_{CO}), 1639 (m, $\nu_{C=C}$).

NMR ($CDCl_3$, δ/ppm): ^{1}H (500 MHz) 5.84−5.76 (m, 6H, C**H**═), 5.02−4.89 (m, 12H, ═C**H$_2$**), 2.05−2.00 (m, 12H, C**H$_2$**CH═), 1.87−1.77 (m, 12H, C**H$_2$**), 1.57−1.50 (m, 12H, C**H$_2$**), 1.45−1.21 (m, 60H, C**H$_2$**); ^{13}C{^{1}H} (125 MHz) 188.2 (dt, $^1J_{RhC}$ = 75.4 Hz, $^2J_{PC}$ = 16.3 Hz, **C**O), 139.2 (s, **C**H═), 114.3 (s, ═**C**H$_2$), 33.9 (s, **C**H$_2$), 31.5 (virtual t,[17] $^3J_{PC}$ = 6.3 Hz, PCH$_2$CH$_2$**C**H$_2$), 29.5 (s, **C**H$_2$), 29.4 (s, **C**H$_2$), 29.3 (s, **C**H$_2$), 29.1 (s, **C**H$_2$), 24.6 (s, **C**H$_2$), 24.5 (virtual t,[17] $^1J_{PC}$ = 13.8 Hz, P**C**H$_2$); ^{31}P{^{1}H} (202 MHz) 16.5 (d, $^1J_{RhP}$ = 115 Hz).

***trans*-Rh(CO)(Cl)[P((CH$_2$)$_6$CH═CH(CH$_2$)$_6$)$_3$P] (3c).** A Schlenk flask was charged with **2c** (1.306 g, 1.458 mmol), Grubbs' catalyst (ca. half of 0.180 g, 0.220 mmol, 15 mol %), and CH_2Cl_2 (800 mL; the resulting solution is 0.0018 M in **2c**), and fitted with a condenser. The solution was stirred. After 24 h, the remaining catalyst was added. The solution was refluxed, and aliquots were periodically monitored by ^{1}H and ^{31}P NMR. After 48 h, the CH═CH$_2$ signals had disappeared. The solvent was removed by oil pump vacuum. The residue was chromatographed on silica gel (2.5 × 10 cm column; TLC monitoring) with hexane/CH_2Cl_2 (2:1 v/v). The solvent was removed from the product containing fractions by oil pump vacuum to give **3c** as a pale yellow oil (0.890 g, 1.09 mmol, 75%, *E*/*Z* mixture). The ^{31}P{^{1}H} and ^{13}C{^{1}H} NMR spectra showed traces of additional species that may be dimers or oligomers.

NMR (C_6D_6, δ/ppm): ^{1}H (300 MHz) 5.40−5.34 (m, 6H, C**H**═), 2.04−2.00 (m, 24H, C**H$_2$**), 1.70−1.67 (m, 12H, C**H$_2$**), 1.34−1.30 (m, 36H, C**H$_2$**); ^{13}C{^{1}H} (75 MHz) 188.3 (dt, $^1J_{RhC}$ = 74.7 Hz, $^2J_{PC}$ = 15.6 Hz, **C**O), 130.5 (s, **C**H═), 31.8 (s, **C**H$_2$), 31.1 (virtual t,[17] $^3J_{PC}$ = 6.9 Hz, PCH$_2$CH$_2$**C**H$_2$), 28.6 (s, **C**H$_2$), 27.7 (s, **C**H$_2$), 26.9 (virtual t,[17] $^1J_{PC}$ = 12.6 Hz, P**C**H$_2$), 25.7 (s, **C**H$_2$); ^{31}P{^{1}H} (121 MHz) 23.8 (d, $^1J_{RhP}$ = 118 Hz, 70%), 22.0 (d, $^1J_{RhP}$ = 124 Hz, 30%).

***trans*-Rh(CO)(Cl)[P((CH$_2$)$_8$CH═CH(CH$_2$)$_8$)$_3$P] (3e).** A Schlenk flask was charged with **2e** (1.511 g, 1.420 mmol) and CH_2Cl_2 (700 mL, the resulting solution is 0.0020 M in **2e**). A solution of Grubbs' catalyst (0.088 g, 0.11 mmol, 7.5 mol %) in CH_2Cl_2 (10 mL) was added via syringe. The mixture was stirred (16 h) and a second equal charge of Grubbs' catalyst was added. The solution was refluxed (16 h). A ^{1}H NMR spectrum (aliquot) showed no residual CH═CH$_2$ signals. The sample was passed through neutral alumina (5.0 × 30 cm column), which was rinsed with additional CH_2Cl_2 (500 mL). Rotary evaporation of the filtrate gave crude **3e** as a dark yellow oil (1.153 g, 1.078 mmol, ∼76%), which was used directly for hydrogenation below.

https://doi.org/10.1021/acs.organomet.1c00708
Organometallics 2022, 41, 733−749

***trans*-Rh(CO)(Cl)[P((CH$_2$)$_{14}$)$_3$P] (4c).** *Procedure A (Scheme 2).* A Fischer-Porter bottle was charged with **3c** (0.890 g, 1.09 mmol), PtO_2 (0.037 g, 0.16 mmol, 15 mol %), THF (15 mL), and H_2 (75 psig). The mixture was stirred (12 h). The solvent was removed by oil pump vacuum. The residue was chromatographed on silica gel (2.5 × 9.0 cm column) with hexane/CH_2Cl_2 (3:1 v/v). The solvent was removed from the yellow fraction by oil pump vacuum to give **4c** as a yellow powder (0.479 g, 0.586 mmol, 54%). DSC ($T_i/T_e/T_p/T_c/T_f$): endotherm, 40.0/55.4/69.6/76.27/76.28 °C; endotherm, 103.5/126.7/134.8/139.2/145.8 °C. TGA: onset of mass loss, 277.6 °C (T_e). Anal. Calcd for $C_{43}H_{84}ClOP_2Rh$: C, 63.18; H, 10.36; Found: C, 62.84; H, 10.00.

Procedure B (Scheme 4). A scintillation vial was charged with $[(CO)_2Rh(\mu\text{-}Cl)]_2$ (0.015 g, 0.038 mmol) and hexanes (5 mL). A solution of P((CH$_2$)$_{14}$)$_3$P (**1c**; 0.050 g, 0.077 mmol) in hexanes (10 mL) was added with stirring. After 16 h, the mixture was passed through a pipette of silica, which was rinsed with hexanes (10 mL) and CH_2Cl_2 (10 mL). The yellow fraction was collected, and the solvent was removed by oil pump vacuum to give **4c** as a yellow solid (0.036 g, 0.044 mmol, 58%). IR (cm^{-1}, powder film): 1946−1949 (s, ν_{CO}, range over multiple measurements). MS:[43] 816 ([**M** − 1]$^+$, 20%), 789 ([**M** − CO]$^+$, 95%), 781 ([**M** − Cl]$^+$, 100%), 747 (90%).

NMR (CD_2Cl_2, δ/ppm): ^{1}H (400 MHz): 1.81−1.79 (m, 12H, C**H**$_2$), 1.67−1.63 (m, 12H, C**H**$_2$), 1.46−1.42 (m, 12H, C**H**$_2$), 1.33−1.30 (m, 48H, C**H**$_2$); ^{13}C{^{1}H} (100 MHz) 188.7 (dt, $^1J_{RhC}$ = 75.0 Hz, $^2J_{PC}$ = 16.0 Hz, **C**O), 30.7 (virtual t,[17] $^3J_{PC}$ = 6.5 Hz, PCH$_2$CH$_2$**C**H$_2$), 28.4 (s, **C**H$_2$), 27.7 (s, **C**H$_2$), 27.4 (s, **C**H$_2$), 27.3 (s, **C**H$_2$), 25.6 (virtual t,[17] $^1J_{PC}$ = 12.9 Hz, P**C**H$_2$), 24.5 (s, **C**H$_2$); ^{31}P{^{1}H} (162 MHz) 19.5 (d, $^1J_{RhP}$ = 118 Hz). Data recorded in $CDCl_3$ and $CDFCl_2$ (−20 °C) are given in the Supporting Information.

***trans*-Rh(CO)(Cl)[P((CH$_2$)$_{18}$)$_3$P] (4e).** A Fischer-Porter bottle was charged with **3e** (1.153 g, 1.078 mmol), PtO_2 (0.037 g, 0.16 mmol, 15 mol %), THF (15 mL), and H_2 (75 psig). The mixture was stirred (12 h). The solvent was removed by oil pump vacuum. The residue was chromatographed on silica gel (2.5 × 30.0 cm column) with hexane/CH_2Cl_2 (3:1 v/v). The solvent was removed from the product containing fractions by rotary evaporation. The oily residue was twice dissolved in CH_2Cl_2, and the solvent was removed by rotary evaporation. This gave **4e** as a yellow waxy solid (0.135 g, 0.137 mmol, 13% from **3e** or 10% from **2e**). Anal. Calcd for $C_{55}H_{108}ClOP_2Rh$: C, 67.01; H, 11.04; Found: C, 67.11; H, 11.12. IR (cm^{-1}, wax film): 1950 (s, ν_{CO}).

NMR ($CDCl_3$, δ/ppm): ^{1}H (500 MHz): 1.88−1.78 (m, 12H, C**H**$_2$), 1.63−1.54 (m, 12H, C**H**$_2$), 1.45−1.36 (m, 12H, C**H**$_2$), 1.36−1.22 (m, 72H, C**H**$_2$); ^{13}C{^{1}H} (125 MHz) 188.4 (dt, $^1J_{RhC}$ = 75.4 Hz, $^2J_{PC}$ = 13.8 Hz, **C**O), 31.2 (virtual t,[17] $^3J_{PC}$ = 6.3 Hz, PCH$_2$CH$_2$**C**H$_2$), 28.8 (s, **C**H$_2$), 28.6 (s, **C**H$_2$), 28.5 (s, **C**H$_2$), 28.3 (s, **C**H$_2$), 28.0 (s, **C**H$_2$), 27.8 (s, **C**H$_2$), 25.1 (virtual t,[17] $^1J_{PC}$ = 13.2 Hz, P**C**H$_2$), 24.7 (s, **C**H$_2$); ^{31}P {^{1}H} (202 MHz) 17.5 (d, $^1J_{RhP}$ = 115 Hz).

***trans*-Rh(CO)(Br)[P((CH$_2$)$_{14}$)$_3$P] (5c).** A scintillation vial was charged with **4c** (0.051 g, 0.062 mmol), NaBr (0.064 g, 0.62 mmol), and CH_2Cl_2 (10 mL). The mixture was vigorously stirred (16 h) and passed through a pipette of Celite, which was rinsed with additional CH_2Cl_2 (5 mL). The solvent was removed from the filtrate by rotary evaporation to give **5c** as a yellow powder (0.052 g, 0.060 mmol, 97%). Anal. Calcd for $C_{43}H_{84}BrOP_2Rh$: C, 60.33; H, 9.90; Found: C, 60.38; H, 10.04. IR (oil film, cm^{-1}): 1944 (s, ν_{CO}). MS:[44] 863 ([**M** + 1]$^+$, ^{81}Br/5%), 861 ([**M** + 1]$^+$, ^{79}Br/5%), 781 ([**M** − Br]$^+$, 100%).

NMR ($CDCl_3$, δ/ppm): ^{1}H (500 MHz) 1.91 (m, 12H, C**H**$_2$), 1.68−1.57 (m, 12H, C**H**$_2$), 1.48−1.38 (m, 12H, C**H**$_2$), 1.38−1.24 (m, 48H, C**H**$_2$); ^{13}C{^{1}H} (126 Hz) 187.7 (dt, $^1J_{RhC}$ = 76.7 Hz, $^2J_{PC}$ = 15.7 Hz, **C**O), 30.5 (virtual t,[17] $^3J_{PC}$ = 6.3 Hz, PCH$_2$CH$_2$**C**H$_2$), 28.1 (s, **C**H$_2$), 27.7 (s, **C**H$_2$), 27.3 (s, **C**H$_2$), 27.2 (s), 26.6 (virtual t,[17] $^1J_{PC}$ = 13.2 Hz, P**C**H$_2$), 24.5 (s, **C**H$_2$); ^{31}P{^{1}H} (202 MHz) 17.5 (d, $^1J_{RhP}$ = 115 Hz).

***trans*-Rh(CO)(I)[P((CH$_2$)$_{14}$)$_3$P] (6c).** *Procedure A (Scheme 2).* An NMR tube was charged with **4c** (0.020 g, 0.025 mmol), NaI (0.015 g, 0.10 mmol), and CD_2Cl_2 (0.8 mL). The mixture was vigorously stirred under N_2 (8 h) and filtered to remove a white solid. The solvent was removed from the filtrate by oil pump vacuum to give **6c** as yellow oil (0.022 g, 0.024 mmol, >95%). The oil was dissolved in CD_2Cl_2, and the solution was layered with methanol. After one week, yellow crystals of **6c** were isolated by filtration (0.010 g, 0.011 mmol, 44%). DSC ($T_i/T_e/T_p/T_c/T_f$): endotherm, 88.0/102.3/104.7/106.4/110.0 °C. TGA: onset of mass loss, 263.8 °C (T_e). Anal. Calcd for $C_{43}H_{84}IOP_2Rh$: C, 56.82; H, 9.32; Found: C, 56.13; H, 9.87.[45]

Procedure B (Scheme 3). Complex **12c** was prepared in an NMR tube (below). Then, N_2 was aspirated through the sample (1 h). A ^{31}P{^{1}H} NMR spectrum showed complete conversion to **6c**. Then, CO was aspirated through the sample (1 h). A ^{31}P{^{1}H} NMR spectrum showed ≥98% conversion to **12c**. IR (cm^{-1}, powder film): 1949 (s, ν_{CO}). MS:[43] 910 ([**M** + 1]$^+$, 35%), 880 ([**M** − CO + 1]$^+$, 90%), 781 ([**M** − I]$^+$, 100%), 747 (90%).

NMR (CD_2Cl_2, δ/ppm): ^{1}H (400 MHz) 1.96−1.94 (m, 12H, C**H**$_2$), 1.62−1.61 (m, 12H, C**H**$_2$), 1.45−1.41 (m, 12H, C**H**$_2$), 1.32−1.29 (m, 48H, C**H**$_2$); ^{13}C{^{1}H} (100 MHz) 186.5 (dt, $^1J_{RhC}$ = 75.0 Hz, $^2J_{PC}$ = 15.0 Hz, **C**O), 30.7 (virtual t,[17] $^3J_{PC}$ = 6.5 Hz, PCH$_2$CH$_2$**C**H$_2$), 28.4 (s, **C**H$_2$), 28.0 (virtual t,[17] $^1J_{PC}$ = 13.5 Hz, P**C**H$_2$), 27.9 (s, **C**H$_2$), 27.6 (s, **C**H$_2$), 27.5(s, **C**H$_2$), 24.7 (s, **C**H$_2$); ^{31}P{^{1}H} (162 MHz) 15.8 (d, $^1J_{RhP}$ = 113 Hz).

***trans*-Rh(CO)(NCS)[P((CH$_2$)$_{14}$)$_3$P] (7c).** A Schlenk tube was charged with **4c** (0.050 g, 0.060 mmol), KSCN (0.030 g, 0.30 mmol), and acetone (5 mL). The mixture was stirred (0.5 h) and filtered through a Celite plug. Most of the acetone was removed from the filtrate under vacuum. The sample was cooled to −20 °C and layered with methanol (2 mL). After 24 h, the precipitate was isolated by filtration, washed with methanol, and dried by oil pump vacuum to give **7c** as a yellow powder (0.037 g, 0.044 mmol, 73%). DSC ($T_i/T_e/T_p/T_c/T_f$): endotherm, 62.3/86.2/92.6/95.6/102.9 °C; exotherm, 191.0/215.3/232.6/246.6/259.5 °C. TGA: onset of mass loss, 176.4 °C (T_e). Anal. Calcd for $C_{44}H_{84}NOP_2RhS$: C, 62.91; H, 10.08, N, 1.67; S, 3.82; Found: C, 62.66; H, 9.91; N, 1.48; S, 3.13. IR (cm^{-1}, powder film): 2084 (vs, ν_{NCS}), 1953 (vs, ν_{CO}). MS:[43] 841 ([**M** + 2]$^+$, 49%), 811 ([**M** − CO]$^+$, 28%), 781 ([**M** − NCS]$^+$, 30%), 747 (15%).

NMR (toluene-d_8, δ/ppm): ^{1}H (400 MHz) 1.90−1.60 (m, 12H, PC**H**$_2$), 1.55−1.25 (m, 72H, C**H**$_2$); ^{13}C{^{1}H}[46] (100 MHz) 31.3 (virtual t,[17] $^3J_{PC}$ = 6.5 Hz, PCH$_2$CH$_2$**C**H$_2$), 30.4 (virtual t,[17] $^3J_{PC}$ = 6.5 Hz, PCH$_2$CH$_2$**C**H$_2$), 28.6 (s, **C**H$_2$), 28.3 (s, **C**H$_2$),[47] 28.2 (s, 2**C**H$_2$),[48] 27.7 (s, **C**H$_2$), 27.6 (s, **C**H$_2$), 27.5 (s, **C**H$_2$),[47] 27.1 (virtual t,[17] $^1J_{PC}$ = 12.7 Hz, P**C**H$_2$), 26.9 (s, **C**H$_2$),[47] 26.8 (virtual t,[17] $^1J_{PC}$ = 12.7 Hz, P**C**H$_2$),[47] 25.5 (s, **C**H$_2$),[47] 24.0 (s, **C**H$_2$); ^{31}P{^{1}H} (162 MHz) 21.0 (d, $^1J_{RhP}$ = 115 Hz).

***trans*-Rh(CO)(Ph)[P((CH$_2$)$_{14}$)$_3$P] (8c).** A scintillation vial was charged with **4c** (0.050 g, 0.062 mmol), THF (4 mL), and $ZnPh_2$ (0.028 g, 0.13 mmol) with stirring. The reaction was monitored by ^{31}P{^{1}H} NMR. After 30 min (complete conversion), EtOH [1 mL; degassed by sparging with N_2 (4 h)] was added. The solvent was removed by oil pump vacuum. The residue was dissolved in toluene (1 mL) and passed through a pipette of silica, which was eluted with additional toluene (5 mL). The solvent was removed from the yellow filtrate by oil pump vacuum. The residue was dissolved in hexanes (4 mL), which was removed by oil pump vacuum. This gave **8c** as a sticky, dark yellow solid (0.047 g, 0.055 mmol, 89%) that decomposed without melting between 110 and 138 °C. Anal. Calcd for $C_{50}H_{91}OP_2Rh$: C, 68.78; H, 10.51; Found: C, 68.43; H, 10.61. IR (powder film, cm^{-1}): 1937 (s, ν_{CO}).

NMR (C_6D_6, δ/ppm): ^{1}H (500 MHz) 7.53 (d, $^3J_{HH}$ = 7.5 Hz, 2H, *o*-C**H**), 7.24 (t, $^3J_{HH}$ = 7.0 Hz, 2H, *m*-C**H**), 7.04 (t, $^3J_{HH}$ = 7.5 Hz, 1H, *p*-C**H**), 2.00−1.90 (br m, 4H, C**H**$_2$), 1.76 (s, 8H, C**H**$_2$), 1.51−1.35 (br m, 66H, C**H**$_2$), 1.20−1.18 (br m, 5H, C**H**$_2$); ^{13}C{^{1}H} (125 MHz) 196.9 (dt, $^1J_{RhC}$ = 55.3 Hz, $^2J_{PC}$ = 13.8 Hz, **C**O), 173.1 (dt, $^1J_{RhC}$ = 26.4 Hz, $^2J_{PC}$ = 16.3, *i*-Ph), 138.8 (t, $^3J_{PC}$ = 3.2 Hz, *o*-Ph), 126.3 (s, *m*-Ph),[50] 122.2 (s, *p*-Ph), 30.5 (virtual t,[17] $^3J_{PC}$ = 6.8 Hz, PCH$_2$CH$_2$**C**H$_2$),[47] 29.9 (virtual t,[17] $^3J_{PC}$ = 6.0 Hz, PCH$_2$CH$_2$**C**H$_2$), 28.6 (s, **C**H$_2$), 28.2 (s, **C**H$_2$), 28.1 (s, **C**H$_2$),[47] 27.9 (virtual t,[17] $^1J_{PC}$ = 11.7 Hz, P**C**H$_2$), 27.7 (s, **C**H$_2$),[47] 27.20 (s, **C**H$_2$), 27.17 (s, **C**H$_2$),[47]

https://doi.org/10.1021/acs.organomet.1c00708
Organometallics 2022, 41, 733−749

27.13 (s, $\underline{C}H_2$), 27.06 (s, $\underline{C}H_2$),[47] 25.9 (virtual t,[17] $^1J_{PC}$ = 12.8 Hz, P$\underline{C}H_2$),[47] 25.0 (s, $\underline{C}H_2$),[47] 23.4 (s, $\underline{C}H_2$); $^{31}P\{^1H\}$ (202 MHz) 17.2 (d, $^1J_{RhP}$ = 142 Hz).

***trans*-Rh(CO)(Me)[P((CH$_2$)$_{14}$)$_3$P] (9c).** A scintillation vial was charged with **4c** (0.050 g, 0.062 mmol), hexanes (10 mL), and MeLi·LiBr (1.5 M in Et_2O; 0.41 mL, 0.62 mmol) with stirring. After 16 h, the solution was passed through a filter syringe.[49] The solvent was removed from the filtrate to give **9c** as a yellow solid (0.046 g, 0.058 mmol, 94%) that was 92% pure by $^{31}P\{^1H\}$ NMR (byproduct peak δ 21.1, d, $^1J_{RhP}$ = 142 Hz). IR (powder film, cm^{-1}): 1929 (s, ν_{CO}).

NMR (C_6D_6, δ/ppm): ^1H (500 MHz) 1.78 (br s, 24H, C$\underline{H}_2$), 1.55−1.41 (br m, 64H, C$\underline{H}_2$), −0.22 (dt, $^2J_{RhH}$ = 1.5 Hz, $^3J_{PH}$ = 8.3 Hz, 3H, C$\underline{H}_3$); $^{13}C\{^1H\}$ (125 MHz) 192.8 (dt, $^1J_{RhC}$ = 56.6 Hz, $^2J_{PC}$ = 15.1 Hz, $\underline{C}O$), 30.8 (virtual t,[17] $^3J_{PC}$ = 7.5 Hz, PCH$_2$CH$_2$$\underline{C}H_2$), 28.1 (s, $\underline{C}H_2$), 27.8 (s, $\underline{C}H_2$) 27.6 (virtual t,[17] $^1J_{PC}$ = 11.3 Hz, P$\underline{C}H_2$) 27.3 (s, $\underline{C}H_2$), 27.1 (s, $\underline{C}H_2$), 25.0 (s, $\underline{C}H_2$), −5.3 (dt, $^1J_{RhC}$ = 20.1 Hz, $^2J_{PC}$ = 13.9 Hz, $\underline{C}H_3$); $^{31}P\{^1H\}$ (202 MHz) 21.6 (d, $^1J_{RhP}$ = 142 Hz).

***trans*-Rh(CO)(H$_2$BH$_2$)[P((CH$_2$)$_{14}$)$_3$P] (10c).** A scintillation vial was charged with **4c** (0.050 g, 0.062 mmol), THF (5 mL), and $NaBH_4$ (0.023 g, 0.62 mmol) with stirring. After 20 h, the sample was filtered through a pipette of alumina, which was rinsed with THF (6 mL). The solvent was removed from the filtrate by oil pump vacuum. The red-brown residue was extracted with hexanes (4 mL) and filtered through a glass microfiber filter paper. The solvent was removed from the filtrate by oil pump vacuum to give **10c** as a beige solid (0.049 g, 0.061 mmol, 99%) that decomposed between 70 and 93 °C without melting. Anal. Calcd for $C_{44}H_{90}BOP_2Rh$: C, 65.18; H, 11.19; Found: C, 64.94; H, 11.09. IR (powder film, cm^{-1}): 2394 (w, ν_{BH}), 1940 (s, ν_{CO}).

NMR (C_6D_6, δ/ppm): ^1H (500 MHz) 1.79−1.76 and 1.73−1.70 (2 br m, 24H, C$\underline{H}_2$), 1.43 (br s, 60H, C$\underline{H}_2$), −0.93 and −1.05 (2 br s, 4H, B$\underline{H}_4$); $^{13}C\{^1H\}$ (125 MHz) 191.8 (dt, $^1J_{RhC}$ = 74.2 Hz, $^2J_{PC}$ = 17.6 Hz, $\underline{C}O$), 30.5 (t, $^3J_{PC}$ = 6.3 Hz, PCH$_2$CH$_2$$\underline{C}H_2$), 28.5 (s, $\underline{C}H_2$), 27.8 (s, $\underline{C}H_2$), 27.7 (s, $\underline{C}H_2$), 27.5 (s, $\underline{C}H_2$), 27.0 (t, $^1J_{PC}$ = 12.6 Hz, P$\underline{C}H_2$), 24.3 (s, $\underline{C}H_2$); $^{31}P\{^1H\}$ (202 MHz) 21.7 (d, $^1J_{RhP}$ = 110 Hz).

***trans*-Rh(CO)(D$_2$BD$_2$)[P((CH$_2$)$_{14}$)$_3$P] (10c-*d*$_4$).** **4c** (0.050 g, 0.062 mmol), THF (5 mL), and $NaBD_4$ (0.026 g, 0.62 mmol) were combined in a procedure analogous to that given for **10c**. An identical workup gave **10c**-d_4 as a beige solid (0.038 g, 0.049 mmol, 79%). Anal. Calcd for $C_{44}H_{86}D_4BOP_2Rh$: C, 64.85; H, 11.63; Found: C, 65.57; H, 11.11. IR (powder film, cm^{-1}): 1940 (s, ν_{CO}), 1749 (w, ν_{BD}). NMR data are largely similar to those of **10c** and given in the Supporting Information.

***trans*-Rh(CO)(Cl)(Br)(CCl$_3$)[P((CH$_2$)$_{14}$)$_3$P] (11c).** An NMR tube was charged with **4c** (0.049 g, 0.067 mmol), $CBrCl_3$ (0.034 mL, 0.34 mmol), and C_6D_6 (1.0 mL). The mixture was stirred (1 h). The volatiles were removed by oil pump vacuum, and the residue was washed with methanol to give **11c** as a pale yellow solid (0.066 g, 0.065 mmol, 97%). DSC: no phase transition below 102.5 °C. TGA: onset of mass loss, 102.5 °C (T_e). Anal. Calcd for $C_{44}H_{84}BrCl_4OP_2Rh$: C, 52.04; H, 8.28; Found: C, 52.01; H, 8.07. IR (cm^{-1}, powder film): 2069 (vs, ν_{CO}). MS:[43] 951 ([**M** − CO − Cl]$^+$, 28%), 907 ([**M** − CO − Br]$^+$, 30%), 869 ([**M** − CO − CCl_3]$^+$ 78%), 823 (100%).

NMR (C_6D_6, δ/ppm): ^1H (400 MHz) 3.10−2.90 (br m, 2H, C$\underline{H}_2$), 2.80−2.60 (br m, 2H, C$\underline{H}_2$), 2.50−2.35 (br m, 4H, C$\underline{H}_2$), 2.30−1.95 (br m, 6H, C$\underline{H}_2$), 1.85−1.65 (br m, 2H, C$\underline{H}_2$), 1.73−1.31 (m, 68H, C$\underline{H}_2$); $^{13}C\{^1H\}$ (100 MHz) 183.0 (dt, $^1J_{RhC}$ = 62.0 Hz, $^2J_{PC}$ = 6.9 Hz, $\underline{C}O$), 87.9 (dt, $^1J_{RhC}$ = 46.6 Hz, $^2J_{PC}$ = 4.0 Hz, $\underline{C}Cl_3$), 30.9 (virtual t,[17] $^3J_{PC}$ = 6.3 Hz, PCH$_2$CH$_2$$\underline{C}H_2$), 30.49 (virtual t,[17] $^3J_{PC}$ = 4.1 Hz, PCH$_2$CH$_2$$\underline{C}H_2$), 30.43 (virtual t,[17] $^3J_{PC}$ = 6.4 Hz, PCH$_2$CH$_2$$\underline{C}H_2$), 30.0 (s, $\underline{C}H_2$), 29.8 (s, $\underline{C}H_2$), 29.2 (s, $\underline{C}H_2$), 29.1 (s, $\underline{C}H_2$), 29.0 (s, $\underline{C}H_2$), 28.9 (s, $\underline{C}H_2$), 28.7 (s, $\underline{C}H_2$), 28.4 (s, $\underline{C}H_2$), 28.3 (s, $\underline{C}H_2$), 28.2 (s, $\underline{C}H_2$), 27.8 (s, $\underline{C}H_2$), 27.2 (s, $\underline{C}H_2$), 26.0 (virtual t,[17] $^1J_{PC}$ = 12.8 Hz, P$\underline{C}H_2$), 25.2 (virtual t,[17] $^1J_{PC}$ = 15.6 Hz, P$\underline{C}H_2$), 23.9 (s, $\underline{C}H_2$), 23.6 (s, $\underline{C}H_2$), 23.3 (s, $\underline{C}H_2$), 22.8 (virtual t,[17] $^1J_{PC}$ = 12.6 Hz, P$\underline{C}H_2$);[26] $^{31}P\{^1H\}$ (162 MHz) 15.6 (d, $^1J_{RhP}$ = 83 Hz). Data recorded in toluene-d_8 (60 °C) are given in the Supporting Information.

***trans*-Rh(CO)$_2$(I)[P((CH$_2$)$_{14}$)$_3$P] (12c).** An NMR tube was charged with **4c** (0.020 g, 0.025 mmol), NaI (0.015 g, 0.1 mmol), and CD_2Cl_2 (0.8 mL) and fitted with a septum. The tube was purged with CO and stirred (4 h) under a balloon pressure of CO. NMR spectra were periodically recorded. After conversion was complete (>98%), the sample was filtered under CO to remove a white solid. The filtrate was saturated with CO and layered with CO-saturated methanol. After 24 h, yellow crystals of **12c** had formed, some of which were collected from the walls of the tube and immediately analyzed. IR (cm^{-1}, powder film): 1988 (m, ν_{CO}), 1930 (s, ν_{CO}).

NMR (CD_2Cl_2, δ/ppm, −40 °C): ^1H (400 MHz) 1.98 (br m, 8H, C$\underline{H}_2$), 1.69 (br m, 4H, C$\underline{H}_2$), 1.54 (br m, 4H, C$\underline{H}_2$), 1.37 (m, 8H, C$\underline{H}_2$), 1.16 (m, 60H, C$\underline{H}_2$); $^{13}C\{^1H\}$ (100 MHz) 192.3 (dt, $^1J_{RhC}$ = 71.5 Hz, $^2J_{PC}$ = 16.0 Hz, $\underline{C}O$), 30.7 (br m, $\underline{C}H_2$), 29.8 (virtual t,[17] $^3J_{PC}$ = 5.6 Hz, PCH$_2$CH$_2$$\underline{C}H_2$),[47] 29.3 (virtual t,[17] $^1J_{PC}$ = 15.6 Hz, P$\underline{C}H_2$),[47] 28.3 (virtual t,[17] $^1J_{PC}$ = 15.6 Hz, P$\underline{C}H_2$), 27.6 (s, $\underline{C}H_2$),[47] 27.4 (s, $\underline{C}H_2$), 27.2 (s, 2$\underline{C}H_2$),[48] 26.1 (s, $\underline{C}H_2$),[47] 26.0 (s, $\underline{C}H_2$),[47] 25.9 (s, $\underline{C}H_2$), 24.9 (s, $\underline{C}H_2$), 24.2 (s, $\underline{C}H_2$), 24.0 (s, $\underline{C}H_2$); $^{31}P\{^1H\}$ (162 MHz) 26.2 (d, $^1J_{RhP}$ = 85 Hz). Data recorded at other temperatures are given in the Supporting Information.

Reaction of 4c and PMe$_3$. A scintillation vial was charged with hexanes (6 mL), **4c** (0.050 g, 0.061 mmol), and PMe_3 (1.0 M in toluene; 0.61 mL, 0.61 mmol) with stirring. After 20 h, the yellow slurry was filtered through glass wool. The wool retained a yellow solid, which was rinsed with hexanes (2 mL). The filtrate was filtered through a pipette of silica gel, which was rinsed with hexanes (15 mL). The solvent was removed from the filtrate by oil pump vacuum to give P((CH$_2$)$_{14}$)$_3$P (**1c**;[7a] 0.023 g, 0.035 mmol, 58%) as a white solid. Then, THF (5 mL) was added to the yellow solid, which extracted it through the glass wool. The solvent was removed from the extract by oil pump vacuum to give *trans*-Rh(CO)(Cl)(PMe$_3$)$_2$ (**13**;[27] 0.014 g, 0.044 mmol, 72%) as a yellow solid. IR (powder film, cm^{-1}): 1952 (s, ν_{CO}).

Data for **1c**:[7a] NMR (C_6D_6, δ/ppm): ^1H (500 MHz) 1.55−1.49, 1.43−1.35 (2 br m, 84H, C$\underline{H}_2$); $^{13}C\{^1H\}$ (125.7 MHz) 31.1 (d, $^3J_{PC}$ = 10.1 Hz, PCH$_2$CH$_2$$\underline{C}H_2$), 29.3 (s, $\underline{C}H_2$), 29.2 (s, $\underline{C}H_2$), 29.2 (s, $\underline{C}H_2$), 28.8 (s, $\underline{C}H_2$), 27.2 (d, $^1J_{PC}$ = 15.1 Hz, P$\underline{C}H_2$), 25.6 (d, $^2J_{PC}$ = 12.6 Hz, $\underline{C}H_2$); $^{31}P\{^1H\}$ (202 MHz) −32.2 (s). IR (powder film, cm^{-1}): 2920 and 2851 (ν_{CH}).

Data for **13**:[27] NMR (C_6D_6, δ/ppm): ^1H (500 MHz) 1.18 (dt, $^2J_{PH}$ = 3.5 Hz, $^3J_{RhH}$ = 1.0 Hz, 18H P(C$\underline{H}_3$)$_3$); $^{13}C\{^1H\}$ (125 MHz) 188.8 (dt, $^1J_{RhC}$ = 75.4 Hz, $^2J_{PC}$ = 16.3 Hz, $\underline{C}O$), 15.2 (dt, $^1J_{PC}$ = 15.1 Hz, $^2J_{RhC}$ = 1.3 Hz, P($\underline{C}H_3$)$_3$); $^{31}P\{^1H\}$ (202 MHz) −10.0 (d, $^1J_{RhP}$ = 115 Hz, $\underline{P}(CH_3)_3$).

Crystallography. A. Crystals of **5c** were obtained by slow evaporation of a THF/pentanes solution derived from a reaction designed to produce **9c** (from **4c** and MeLi·LiBr). Data were collected as summarized in Table 1. Integrated intensity information for each reflection was obtained by reduction of the data frames with the program APEX2.[51] Data were corrected for Lorentz and polarization factors as well as for crystal decay using the program SADABS.[52] The structure was solved using SHELXTL.[53] Non-hydrogen atoms were refined with anisotropic thermal parameters. The hydrogen atoms were placed in idealized positions and refined using a riding model. The structure was refined (weighted least squares refinement on F^2) to convergence.[52]

B. An NMR tube was charged under N_2 with a solution of **6c** (0.010 g) in benzene/CH_2Cl_2 (1:1 v/v; 0.2 mL), which was layered with methanol (2.0 mL). After 14 d, data were collected on the yellow prisms as outlined in Table 1. Cell parameters were obtained from 10 frames using a 10° scan and refined with 10410 reflections. Lorentz, polarization, and absorption corrections[54] were applied. The structure was solved by direct methods. The parameters were refined with all data by full-matrix-least-squares on F^2 using SHELXL-97.[53] Non-hydrogen and hydrogen atoms were treated as for **5c**. Scattering factors were taken from literature.[55] The I−Rh−CO moiety was disordered, with two orientations differing by ca. 180°. The iodine

https://doi.org/10.1021/acs.organomet.1c00708
Organometallics 2022, 41, 733−749

atoms refined to an 89:11 occupancy ratio (I1/I1′), but the CO associated with the minor rotamer (coincident with the iodine of the major rotamer) could not be resolved. The atom C54 was also disordered and could be refined to a 65:35 occupancy ratio (C54/C54′). The anisotropic displacement parameters of neighboring atoms (e.g., C55, C56) indicated further disorder that could not be resolved.

C. Crystals of **8c** were obtained from a solution of nitromethane, CH_2Cl_2, and pentanes. Data were collected as summarized in Table 1 and treated as described for **5c**. The structure solved readily in the non-centrosymmetric space group $P2_1$ (no. 33) using the charge flipping algorithm implemented in PLATON.[56] Non-hydrogen and hydrogen atoms were treated as for **5c**. The thermal ellipsoids associated with C1 to C14 indicated disorder, but this could not be successfully modeled, so the ellipsoids were restrained. The structure was refined (weighted least squares refinement on F^2) to convergence.[52] The batch scale factor (0.01 with TWIN) confirmed the non-centrosymmetric space group. The Flack parameter (−0.01(4); theory for correct and inverted structures, 0 and 1)[57] verified the absolute configuration.

D. Crystals of **10c** were obtained by layering a CH_2Cl_2 solution with nitromethane in an NMR tube, and then storage at −39 °C. Data were collected as summarized in Table 1 and treated as described for **5c**. The structure was solved analogously. The thermal ellipsoids associated with C1 to C14 indicated disorder, but this could not be successfully modeled, so the ellipsoids were restrained.

■ ASSOCIATED CONTENT

Supporting Information

The Supporting Information is available free of charge at https://pubs.acs.org/doi/10.1021/acs.organomet.1c00708.

Additional NMR and crystallographic data (PDF)

Accession Codes

CCDC 1419504 (**5c**), 602258 (**6c**), 1419505 (**8c**), and 1419503 (**10c**) contain the supplementary crystallographic data for this paper. These data can be obtained free of charge via www.ccdc.cam.ac.uk/data_request/cif, or by emailing data_request@ccdc.cam.ac.uk, or by contacting the Cambridge Crystallographic Data Centre, 12 Union Road, Cambridge CB2 1EZ, U.K.; fax: +44 1123 336033.

■ AUTHOR INFORMATION

Corresponding Author

John A. Gladysz − *Department of Chemistry, Texas A&M University, College Station, Texas 77842-3012, United States;* orcid.org/0000-0002-7012-4872; Email: gladysz@mail.chem.tamu.edu

Authors

Alexander L. Estrada − *Department of Chemistry, Texas A&M University, College Station, Texas 77842-3012, United States*

Leyong Wang − *Institut für Organische Chemie and Interdisciplinary Center for Molecular Materials, Friedrich-Alexander-Universität Erlangen-Nürnberg, 91054 Erlangen, Germany;* Present Address: School of Chemistry and Chemical Engineering, Nanjing University, Nanjing 210023, China; orcid.org/0000-0001-5775-3714

Nattamai Bhuvanesh − *Department of Chemistry, Texas A&M University, College Station, Texas 77842-3012, United States*

Frank Hampel − *Institut für Organische Chemie and Interdisciplinary Center for Molecular Materials, Friedrich-Alexander-Universität Erlangen-Nürnberg, 91054 Erlangen, Germany;* Present Address: Department of Chemistry and Pharmacy, Raum Chemikum, Nikolaus-Fiebiger-Str. 10, 91058 Erlangen, Germany

Complete contact information is available at: https://pubs.acs.org/10.1021/acs.organomet.1c00708

Notes

The authors declare no competing financial interest.

■ ACKNOWLEDGMENTS

The authors thank the US National Science Foundation (CHE-1566601 and CHE-1900549) for support, Dr. Takanori Shima and Tiezheng Jia for preliminary observations, and Prof. Janet Blümel for helpful discussions.

■ REFERENCES

(1) Reviews: (a) Kottas, G. S.; Clarke, L. I.; Horinek, D.; Michl, J. Artificial Molecular Rotors. *Chem. Rev.* **2005**, *105*, 1281−1376. (b) Ehnbom, A.; Gladysz, J. A. Gyroscopes and the Chemical Literature, 2002-2020: Approaches to a Nascent Family of Molecular Devices. *Chem. Rev.* **2021**, *121*, 3701−3750.

(2) Lead references to additional groups active in this area: (a) Howe, M. E.; Garcia-Garibay, M. A. The Roles of Intrinsic Barriers and Crystal Fluidity in Determining the Dynamics of Crystalline Molecular Rotors and Molecular Machines. *J. Org. Chem.* **2019**, *84*, 9835−9849. (b) Tsuchiya, T.; Inagaki, Y.; Yamaguchi, K.; Setaka, W. Structure and Dynamics of Crystalline Molecular Gyrotops with a Difluorophenylene Rotor. *J. Org. Chem.* **2021**, *86*, 2423−2430. (c) Jin, M.; Ando, R.; Jellen, M. J.; Garcia-Garibay, M. A.; Ito, H. Encapsulating *N*-Heterocyclic Carbene Binuclear Transition-Metal Complexes as a New Platform for Molecular Rotation in Crystalline Solid-State. *J. Am. Chem. Soc.* **2021**, *143*, 1144−1153.

(3) (a) Sclater, N.; Chironis, N. P. Gears: Devices, Drives and Mechanisms. *Mechanisms and Mechanical Devices Sourcebook*, 4th ed.; McGraw-Hill, 2007; pp 121−170. (b) Neugebauer, G. H. Gyroscopic Elements. In *Gyroscopes: Theory and Design*; Savet, P. H., Ed.; McGraw-Hill: New York, 1961; Chapter 10.6. (c) Wrigley, W.; Hollister, W. M.; Denhard, W. G. *Gyroscopic Theory, Design, and Instrumentation*; M.I.T. Press, 1969; pp 298−371.

(4) (a) Koen, E.; Pourahmadi, F.; Terry, S. A Multilayer Ceramic Package for Silicon Micromachined Accelerometers. *Proceedings of the International Solid-State Sensors and Actuators Conference—Transducers '95*; Royal Swedish Academy of Engineering Sciences: Stockholm, 1995; pp 273−276. (b) Li, G.; Tseng, A. A. Low Stress Packaging of a Micromachined Accelerometer. *IEEE Trans. Electron. Packag. Manuf.* **2001**, *24*, 18−25. (c) Yazdi, N.; Ayazi, F.; Najafi, K. Micromachined Inertial Sensors. *Proc. IEEE* **1998**, *86*, 1640−1659.

(5) (a) Lang, G. M.; Shima, T.; Wang, L.; Cluff, K. J.; Skopek, K.; Hampel, F.; Blümel, J.; Gladysz, J. A. Gyroscope-Like Complexes Based on Dibridgehead Diphosphine Cages That Are Accessed by Three-Fold Intramolecular Ring Closing Metatheses and Encase $Fe(CO)_3$, $Fe(CO)_2(NO)^+$, and $Fe(CO)_3(H)^+$ Rotators. *J. Am. Chem. Soc.* **2016**, *138*, 7649−7663. (b) Lang, G. M.; Skaper, D.; Hampel, F.; Gladysz, J. A. Synthesis, reactivity, structures, and dynamic properties of gyroscope like iron complexes with dibridgehead diphosphine cages: pre- vs. post-metathesis substitutions as routes to adducts with neutral dipolar Fe(CO)(NO)(X) rotors. *Dalton Trans.* **2016**, *45*, 16190−16204.

(6) (a) Fiedler, T.; Bhuvanesh, N.; Hampel, F.; Reibenspies, J. H.; Gladysz, J. A. Gyroscope like molecules consisting of trigonal or square planar osmium rotators within three-spoked dibridgehead diphosphine stators: syntheses, substitution reactions, structures, and dynamic properties. *Dalton Trans.* **2016**, *45*, 7131−7147. (b) Hess, G. D.; Fiedler, T.; Hampel, F.; Gladysz, J. A. Octahedral Gyroscope-like Molecules Consisting of Rhenium Rotators within Cage-like Dibridgehead Diphosphine Stators: Syntheses, Substitution Reactions,

Structures, and Dynamic Properties. *Inorg. Chem.* **2017**, *56*, 7454−7469.

(7) (a) Nawara-Hultzsch, A. J.; Stollenz, M.; Barbasiewicz, M.; Szafert, S.; Lis, T.; Hampel, F.; Bhuvanesh, N.; Gladysz, J. A. Gyroscope-Like Molecules Consisting of PdX_2/PtX_2 Rotators within Three-Spoke Dibridgehead Diphosphine Stators: Syntheses, Substitution Reactions, Structures, and Dynamic Properties. *Chem.—Eur. J.* **2014**, *20*, 4617−4637. (b) Kharel, S.; Joshi, H.; Bhuvanesh, N.; Gladysz, J. A. Syntheses, Structures, and Thermal Properties of Gyroscope-like Complexes Consisting of $PtCl_2$ Rotators Encased in Macrocyclic Dibridgehead Diphosphines $P((CH_2)_n)_3P$ with Extended Methylene Chains (n = 20/22/30) and Isomers Thereof. *Organometallics* **2018**, *37*, 2991−3000.

(8) (a) Setaka, W.; Inoue, K.; Higa, S.; Yoshigai, S.; Kono, H.; Yamaguchi, K. Synthesis of Crystalline Molecular Gyrotops and Phenylene Rotation inside the Cage. *J. Org. Chem.* **2014**, *79*, 8288−8295 and earlier work cited therein. (b) Setaka, W.; Higa, S.; Yamaguchi, K. Ring-closing metathesis for the synthesis of a molecular gyrotop. *Org. Biomol. Chem.* **2014**, *12*, 3354−3357. (c) Shionari, H.; Inagaki, Y.; Yamaguchi, K.; Setaka, W. A pyrene-bridged macrocage showing no excimer fluorescence. *Org. Biomol. Chem.* **2015**, *13*, 10511−10516. (d) Nishiyama, Y.; Inagaki, Y.; Yamaguchi, K.; Setaka, W. 1,4-Naphthalenediyl-Bridged Molecular Gyrotops: Rotation of the Rotor and Fluorescence in Solution. *J. Org. Chem.* **2015**, *80*, 9959−9966. (e) Masuda, T.; Arase, J.; Inagaki, Y.; Kawahata, M.; Yamaguchi, K.; Ohhara, T.; Nakao, A.; Momma, H.; Kwon, E.; Setaka, W. Molecular Gyrotops with a Five-Membered Heteroaromatic Ring: Synthesis, Temperature-Dependent Orientation of Dipolar Rotors inside the Crystal, and its Birefringence Change. *Cryst. Growth Des.* **2016**, *16*, 4392−4401. (f) Fujiwara, A.; Inagaki, Y.; Momma, H.; Kwon, E.; Yamaguchi, K.; Kanno, M.; Kono, H.; Setaka, W. A crystalline molecular gyrotop with a biphenylene dirotor and its temperature-dependent birefringence. *CrystEngComm.* **2017**, *19*, 6049−6056. (g) Takashima, H.; Inagaki, Y.; Momma, H.; Kwon, E.; Yamaguchi, K.; Setaka, W. Ferrocene-diyl Bridged Macrocages: Steric Effects of the Cage on the Redox Properties of Ferrocene Moiety. *Organometallics* **2018**, *37*, 1501−1506. (h) Hashimoto, H.; Inagaki, Y.; Momma, H.; Kwon, E.; Setaka, W. Kinetic Stabilization of Carbazole Nitroxides by Inclusion in a Macrocage and Their Electron Spin Resonance Characterization. *J. Org. Chem.* **2019**, *84*, 11783−11789. (i) Hashimoto, H.; Inagaki, Y.; Momma, H.; Kwon, E.; Yamaguchi, K.; Setaka, W. Polarized fluorescence of a crystal having uniaxially oriented molecules by a carbazole-diyl-bridged macrocage. *CrystEngComm.* **2019**, *21*, 3910−3914. (j) Inagaki, Y.; Ueda, S.; Yamaguchi, K.; Setaka, W. A Furan-2,5-diyl Bridged Macrocage as a Highly Distorted Molecular Gyrotop. *Chem. Lett.* **2020**, *49*, 1291−1293.

(9) (a) Taher, D.; Nawara-Hultzsch, A. J.; Bhuvanesh, N.; Hampel, F.; Gladysz, J. A. Mono- and disubstitution reactions of gyroscope like complexes derived from Cl-Pt-Cl rotators within cage like dibridgehead diphosphine ligands. *J. Organomet. Chem.* **2016**, *821*, 136−141. (b) Zhu, Y.; Ehnbom, A.; Fiedler, T.; Shu, Y.; Bhuvanesh, N.; Hall, M. B.; Gladysz, J. A. Platinum(ii) alkyl complexes of chelating dibridgehead diphosphines $P((CH_2)_n)_3P$ (n = 14, 18, 22); facile *cis*/*trans* isomerizations interconverting gyroscope and parachute like adducts. *Dalton Trans.* **2021**, *50*, 12457−12477.

(10) Kharel, S.; Joshi, H.; Bierschenk, S.; Stollenz, M.; Taher, D.; Bhuvanesh, N.; Gladysz, J. A. Homeomorphic Isomerization as a Design Element in Container Molecules; Binding, Displacement, and Selective Transport of MCl_2 Species (M = Pt, Pd, Ni). *J. Am. Chem. Soc.* **2017**, *139*, 2172−2175.

(11) (a) Bermudez, V.; Capron, N.; Gase, T.; Gatti, F. G.; Kajzar, F.; Leigh, D. A.; Zerbetto, F.; Zhang, S. Influencing intramolecular motion with an alternating electric field. *Nature* **2000**, *406*, 608−611. (b) Vacek, J.; Michl, J. Molecular dynamics of a grid-mounted molecular dipolar rotor in a rotating electric field. *Proc. Natl. Acad. Sci. U.S.A.* **2001**, *98*, 5481−5486. (c) Horinek, D.; Michl, J. Molecular Dynamics Simulation of an Electric Field Driven Dipolar Molecular Rotor Attached to a Quartz Glass Surface. *J. Am. Chem. Soc.* **2003**, *125*, 11900−11910. (d) Zheng, X.; Mulcahy, M. E.; Horinek, D.; Galeotti, F.; Magnera, T. F.; Michl, J. Dipolar and Nonpolar Altitudinal Molecular Rotors Mounted on an Au(111) Surface. *J. Am. Chem. Soc.* **2004**, *126*, 4540−4542. (e) Horinek, D.; Michl, J. Surface-mounted altitudinal molecular rotors in alternating electric field: Single-molecule parametric oscillator molecular dynamics. *Proc. Natl. Acad. Sci. U.S.A.* **2005**, *102*, 14175−14180. (f) Horansky, R. D.; Clarke, L. I.; Price, J. C.; Khuong, T.-A. V.; Jarowski, P. D.; Garcia-Garibay, M. A. Dielectric response of a dipolar molecular rotor crystal. *Phys. Rev. B: Condens. Matter Mater. Phys.* **2005**, *72*, 014302 (article number). (g) Horansky, R. D.; Clarke, L. I.; Winston, E. B.; Price, J. C.; Karlen, S. D.; Jarowski, P. D.; Santillan, R.; Garcia-Garibay, M. A. Dipolar rotor-rotor interactions in a difluorobenzene molecular rotor crystal. *Phys. Rev. B: Condens. Matter Mater. Phys.* **2006**, *74*, 054306 (article number). (h) de Jonge, J. J.; Ratner, M. A.; de Leeuw, S. W. Local Field Controlled Switching in a One-Dimensional Dipolar Array. *J. Phys. Chem. C* **2007**, *111*, 3770−3777. (i) Vacek, J.; Michl, J. Artificial Surface-Mounted Molecular Rotors: Molecular Dynamics Simulations. *Adv. Funct. Mater.* **2007**, *17*, 730−739. (j) Horansky, R. D.; Magnera, T. F.; Price, J. C.; Michl, J. Artificial Dipolar Molecular Rotors. *Controlled Nanoscale Motion*; Springer, 2007, *711*, 303−330. (k) Arcenegui, J. J.; García-Sánchez, P.; Morgan, H.; Ramos, A. Electric-field-induced rotation of Brownian metal nanowires. *Phys. Rev. E: Stat., Nonlinear, Soft Matter Phys.* **2013**, *88*, 033025 (article number). (l) Zhao, K.; Dron, P. I.; Kaleta, J.; Rogers, C. T.; Michl, J. Arrays of Dipolar Molecular Rotors in Tris(o-phenylenedioxy)-cyclotriphosphazene. *Top. Curr. Chem.* **2014**, *354*, 163−211. (m) Abolins, B. P.; Zillich, R. E.; Whaley, K. B. Quantum phases of dipolar rotors on two-dimensional lattices. *J. Chem. Phys.* **2018**, *148*, 102338 (article number). (n) Kopperger, E.; List, J.; Madhira, S.; Rothfischer, F.; Lamb, D. C.; Simmel, F. C. A self-assembled nanoscale robotic arm controlled by electric fields. *Science* **2018**, *359*, 296−301.

(12) For crystallographically characterized examples, see (a) Dixon, F. M.; Eisenberg, A. H.; Farrell, J. R.; Mirkin, C. A.; Liable-Sands, L. M.; Rheingold, A. L. Neutral Macrocycles via Halide-Induced Ring Opening of Binuclear Condensed Intermediates. *Inorg. Chem.* **2000**, *39*, 3432−3433. (b) Koshevoy, I. O.; Sizova, O. V.; Tunik, S. P.; Lough, A.; Poë, A. J. A Novel Five-Coordinate Rhodium(I) Complex. *Eur. J. Inorg. Chem.* **2005**, 4516−4520.

(13) *Rhodium Catalysis in Organic Synthesis: Methods and Reactions*; Tanaka, K., Ed.; Wiley-VCH: Weinheim, Germany, 2019.

(14) (a) Wang, L.; Shima, T.; Hampel, F.; Gladysz, J. A. Gyroscope-like molecules consisting of three-spoke stators that enclose "switchable" neutral dipolar rhodium rotators; reversible cycling between faster and slower rotating Rh(CO)I and $Rh(CO)_2I$ species. *Chem. Commun.* **2006**, 4075−4077. (b) Estrada, A. L.; Jia, T.; Bhuvanesh, N.; Blümel, J.; Gladysz, J. A. Substitution and Catalytic Chemistry of Gyroscope-Like Complexes Derived from Cl-Rh-CO Rotators and Triply *trans* Spanning Di(trialkylphosphine) Ligands. *Eur. J. Inorg. Chem.* **2015**, 5318−5321.

(15) (a) Dunbar, K. R.; Haefner, S. C. Crystallographic disorder in the orthorhombic form of carbonyl(chlorobis(triphenylphosphine)-rhodium: relevance to the reported structure of the paramagnetic impurity in Wilkinson's catalyst. *Inorg. Chem.* **1992**, *31*, 3676−3679. (b) Guillevic, M.-A.; Rocaboy, C.; Arif, A. M.; Horváth, I. T.; Gladysz, J. A. Organometallic Reactivity Patterns in Fluorocarbons and Implications for Catalysis: Synthesis, Structure, Solubility, and Oxidative Additions of a Fluorous Analogue of Vaska's Complex, *trans*-$Ir(CO)(Cl)[P(CH_2CH_2(CF_2)_5CF_3)_3]_2$. *Organometallics* **1998**, *17*, 707−717.

(16) Nawara-Hultzsch, A. J.; Skopek, K.; Shima, T.; Barbasiewicz, M.; Hess, G. D.; Skaper, D.; Gladysz, J. A. Syntheses and Palladium, Platinum, and Borane Adducts of Symmetrical Trialkylphosphines with Three Terminal Vinyl Groups, $P((CH_2)_mCH{=}CH_2)_3$. *Z. Naturforsch.* **2010**, *65*, 414−424.

(17) (a) Hersh, W. H. False AA'X Spin-Spin Coupling Systems in 13C NMR: Examples Involving Phosphorus and a 20-Year-Old Mystery in Off-Resonance Decoupling. *J. Chem. Educ.* **1997**, *74*,

1485−1488. (b) The $^{n}JP_{C}$ values given herein represent the apparent coupling between adjacent peaks of the virtual triplet, with *n* designating the number of bonds between the carbon atom and the closest phosphorus atom in the spin system.

(18) However, a trigonal pyramidal iron complex of the same phosphine, *trans*-$Fe(CO)_3(P((CH_2)_5CH{=}CH_2)_3)_2$, gives a gyroscope like product in high yield.[5a] This difference can be rationalized by conformational considerations.[1b,5a]

(19) Representative examples from an extensive literature: (a) Sough, G. A.; Bergman, R. G.; Heathcock, C. H. Synthesis of η^1 Oxygen-Bound Rhodium Enolates. Applications to Catalytic Aldol Chemistry. *J. Am. Chem. Soc.* **1989**, *111*, 938−949. (b) Moigno, D.; Kiefer, W.; Callejas-Gaspar, B.; Gil-Rubio, J.; Werner, H. Metal-carbon vibrational modes as a probe of the $_{trans}$ influence in vinylidene and carbonyl rhodium(I) complexes. *New J. Chem.* **2001**, *25*, 1389−1397. (c) Cheliatsidou, P.; White, D. F. S.; Slawin, A. M. Z.; Cole-Hamilton, D. J. Modelling proposed intermediates in the hydrocarbonylation of alkenes catalysed by rhodium complexes of PBu^i_3 and PPr^i_3. *Dalton Trans.* **2008**, 2389−2394.

(20) (a) Jennings, M. A.; Wojcicki, A. Thiocyanato Complexes of Rhodium(I). *Inorg. Chem.* **1967**, *6*, 1854−1859. (b) An isomeric RhSCN species should exhibit an IR ν_{SCN} value of >2110 cm^{-1}. (c) Blake, A. J.; Ebsworth, E. A. V.; Watson, P. G. Structure of *trans*-carbonyl(thiocyanato-*N*)bis(triethylphosphine)rhodium(I). *Acta Crystallogr., Sect. C: Cryst. Struct. Commun.* **1993**, *49*, 1773−1775.

(21) (a) Marks, T. J.; Kolb, J. R. Covalent Transition Metal, Lanthanide, and Actinide Tetrahydroborate Complexes. *Chem. Rev.* **1977**, *77*, 263−293. (b) Besora, M.; Lledós, A. Coordination Modes and Hydride Exchange Dynamics in Transition Metal Tetrahydroborate Complexes. Contemporary Metal Boron Chemistry I. *Structure and Bonding*; Springer, 2008; Vol. *130*, pp 149−202.

(22) Representative examples involving rhodium: (a) Shafiq, F.; Eisenberg, R. Binuclear Rhodium Hydride Complexes: Synthesis, Structure, and Reactivity. *Inorg. Chem.* **1993**, *32*, 3287−3294. (b) Nückel, S.; Burger, P. Transition Metal Complexes with Sterically Demanding Ligands, 3.1 Synthetic Access to Square-Planar Terdentate Pyridine−Diimine Rhodium(I) and Iridium(I) Methyl Complexes: Successful Detour via Reactive Triflate and Methoxide Complexes. *Organometallics* **2001**, *20*, 4345−4359.

(23) Nakamoto, K. *Infrared and Raman Spectra of Inorganic and Coordination Compounds, Part A, Theory and Applications in Inorganic Chemistry*, 6th ed.; John Wiley & Sons: Hoboken, New Jersey, 2009; Chapter 2.

(24) (a) Segal, B. G.; Lippard, S. J. Transition metal hydroborate complexes. 9. Preparation, properties, and structure of di-μ-cyanotrihydroborato-bis(2,2′,2′′-triaminotriethylamine) dinickel(II) tetraphenylborate. *Inorg. Chem.* **1977**, *16*, 1623−1629. (b) Desrochers, P. J.; LeLievre, S.; Johnson, R. J.; Lamb, B. T.; Phelps, A. L.; Cordes, A. W.; Gu, W.; Cramer, S. P. A Stable Monomeric Nickel Borohydride. *Inorg. Chem.* **2003**, *42*, 7945−7950. (c) Desrochers, P. J.; Sutton, C. A.; Abrams, M. L.; Ye, S.; Neese, F.; Telser, J.; Ozarowski, A.; Krzystek, J. Electronic Structure of Nickel(II) and Zinc(II) Borohydrides from Spectroscopic Measurements and Computational Modeling. *Inorg. Chem.* **2012**, *51*, 2793−2805. (d) Bonanno, J. B.; Henry, T. P.; Wolczanski, P. T.; Pierpont, A. W.; Cundari, T. R. Evidence for Strong Tantalum-to-Boron Dative Interactions in $(silox)_3Ta(BH_3)$ and $(silox)_3Ta(\eta^2\text{-B,Cl-}BCl_2Ph)$ (silox = $^tBu_3SiO$). *Inorg. Chem.* **2007**, *46*, 1222−1232.

(25) (a) Cable, C. J.; Adams, H.; Bailey, N. A.; Crosby, J.; White, C. Does the rhodium-catalysed addition of perhaloalkanes to alkenes (i.e. the Kharasch reaction) proceed via an oxidative-addition mechanism?: the crystal structure of $RhBr(CCl_3)Cl(CO)(PMe_3)_2$. *J. Chem. Soc., Chem. Commun.* **1991**, 165−166. (b) Scott, S. L.; Szpakowicz, M.; Mills, A.; Santini, C. C. Ligand Exchange and Oxidative Addition on a Silica-Supported Rhodium Complex, *trans*-$[(\equiv SiO)Rh(PMe_3)_2(CO)]$. *J. Am. Chem. Soc.* **1998**, *120*, 1883−1890.

(26) Two of the three triplets expected for the PCH_2 signals are prominent in Figure 2 (26.0, 25.2 ppm, $^1J_{PC}$ = 12.8, 15.6 Hz), but the third (22.8 ppm, $^1J_{PC}$ = 12.6 Hz) is much less intense (albeit reproducible). Hence, the 22.8 ppm assignment is considered tentative.

(27) Boyd, S. E.; Field, L. D.; Hambley, T. W.; Partridge, M. G. Synthesis and characterization of $Rh[P(CH_3)_3]_2(CO)CH_3$ and $Rh[P(CH_3)_3]_2(CO)Ph$. *Organometallics* **1993**, *12*, 1720−1724.

(28) In a separate experiment, spectra were recorded at −80 °C after the addition of each aliquot (at room temperature). Small quantities of **1c** were now apparent after the first equivalent.

(29) Choi, J.-C.; Sakakura, T. Oxidative Addition of C−H Bonds to $RhCl(PMe_3)_3$: Relevant to the Catalytic Transformation of Hydrocarbons. *J. Am. Chem. Soc.* **2003**, *125*, 7762−7763 (see page s2 of their SI).

(30) (a) Bondi, A. van der Waals Volumes and Radii. *J. Phys. Chem.* **1964**, *68*, 441−451. (b) Mantina, M.; Chamberlin, A. C.; Valero, R.; Cramer, C. J.; Truhlar, D. G. Consistent van der Waals Radii for the Whole Main Group. *J. Phys. Chem. A* **2009**, *113*, 5806−5812. (c) The values used for this study are as follows (Å): H, 1.10; B, 1.92; C, 1.70; N, 1.55; O, 1.52; S, 1.80; Cl, 1.75; Br, 1.83; I, 1.98.

(31) Lang, G. M.; Bhuvanesh, N.; Reibenspies, J. H.; Gladysz, J. A. Syntheses, Reactivity, Structures, and Dynamic Properties of Gyroscope-like Iron Carbonyl Complexes Based on Dibridgehead Diarsine Cages. *Organometallics* **2016**, *35*, 2873−2889.

(32) (a) Anslyn, E. V.; Dougherty, D. A. *Modern Physical Organic Chemistry*; University Science Books: Sausalito, California, 2006; pp 97−98. (b) Eliel, E. N.; Wilen, S. H. *Stereochemistry of Organic Compounds*; John Wiley & Sons: New York, 1994; pp 6241142−6291155.

(33) For additional comparisons involving unsymmetrically substituted platinum complexes (X−Pt−Y), see ref 9a.

(34) Stollenz, M.; Barbasiewicz, M.; Nawara-Hultzsch, A. J.; Fiedler, T.; Laddusaw, R. M.; Bhuvanesh, N.; Gladysz, J. A. Dibridgehead Diphosphines that Turn Themselves Inside Out. *Angew. Chem., Int. Ed.* **2011**, *50*, 6647−6651; Dreifach-verbrückte Diphosphane mit von innen nach au*ß*en invertierender Konfiguration. *Angew. Chem.* **2011**, *123*, 6777−6781.

(35) (a) Park, C. H.; Simmons, H. E. Macrobicyclic amines. II. out-out in-in Prototropy in 1,(k + 2)-diazabicyclo[k.l.m]alkaneammonium ions. *J. Am. Chem. Soc.* **1968**, *90*, 2429−2431 See also the immediately preceding and following communications. (b) Alder, R. W.; East, S. P. In/Out Isomerism. *Chem. Rev.* **1996**, *96*, 2097−2112.

(36) Ehnbom, A.; Kuszynski, J. E.; Hall, M. B.; Gladysz, J. A. A Computational Investigation of Structure, Energetics, Interconversion, and NMR Properties of Macrocyclic Aliphatic Dibridgehead Diphosphines Exhibiting In/Out Isomerism. manuscript in preparation.

(37) Zurakowski, J. A.; Austen, B. J. H.; Drover, M. W. Wrapping Rhodium in a Borane Canopy: Implications for Hydride Formation and Transfer. *Organometallics* **2021**, *40*, 2450−2457.

(38) (a) Leforestier, B.; Gyton, M. R.; Chaplin, A. B. Synthesis and group 9 complexes of macrocyclic PCP and POCOP pincer ligands. *Dalton Trans.* **2020**, *49*, 2087−2101. (b) Leforestier, B.; Gyton, M. R.; Chaplin, A. B. Oxidative Addition of a Mechanically Entrapped C(sp)-C(sp) Bond to a Rhodium(I) Pincer Complex. *Angew. Chem., Int. Ed.* **2020**, *59*, 23500−23504; *Angew. Chem.* **2020**, *132*, 23706−23710.

(39) Jongkind, L. J.; Reek, J. N. H. Asymmetric Hydroformylation Using a Rhodium Catalyst Encapsulated in a Chiral Capsule. *Chem.—Asian J.* **2020**, *15*, 867−875.

(40) Rodriguez-Molina, B.; Ochoa, M. E.; Farfán, N.; Santillan, R.; García-Garibay, M. A. Synthesis, Characterization, and Rotational Dynamics of Crystalline Molecular Compasses with N-Heterocyclic Rotators. *J. Org. Chem.* **2009**, *74*, 8554−8565 and earlier work cited therein.

(41) Siegel, J. S.; Anet, F. A. L. Dichlorofluoromethane-*d*: A Versatile Solvent for VT-NMR Experiments. *J. Org. Chem.* **1988**, *53*, 2629−2630.

(42) Cammenga, H. K.; Epple, M. Basic Principles of Thermoanalytical Techniques and Their Applications in Preparative Chemistry. *Angew. Chem., Int. Ed. Engl.* **1995**, *34*, 1171−1187; Grundlagen der

Thermischen Analysetechniken und ihre Anwendungen in der präparativen Chemie. *Angew. Chem.* **1995**, *107*, 1284−1301.
(43) FAB MS, 3-NBA, *m/z* (relative intensity, %); the most intense peak of isotope envelope is given.
(44) +ESI MS, *m/z* (relative intensity, %); the most intense peak of isotope envelope.
(45) Although a few compounds did not give satisfactory microanalyses, the best available data are given.
(46) The **CO** and **NCS** signals were not observed.
(47) These signals were more intense than the others (ca. 2:1 area ratios).
(48) The signal represents two overlapping carbons of the unique bridge.
(49) The commercial product used: https://us.vwr.com/store/product/4830563/vwr-syringe-filters.
(50) The ^{13}C NMR signal with the chemical shift closest to benzene is assigned to the meta carbon atom; Mann, B. E. The Carbon-13 and Phosphorus-31 Nuclear Magnetic Resonance Spectra of Some Tertiary Phosphines. *J. Chem. Soc., Perkin Trans. 2* **1972**, 30−34.
(51) *APEX2 "Program for Data Collection on Area Detectors"*; BRUKER AXS Inc., 5465 East Cheryl Parkway; Madison, WI 53711-5373 USA.
(52) Sheldrick, G. M. *SADABS (Version 2008/1): Program for Absorption Correction of Area Detector Frames*. 5465 East Cheryl Parkway; BRUKER AXS Inc.: Madison, WI 53711-5373 USA.
(53) (a) Sheldrick, G. M. SHELXT- Integrated space-group and crystal-structure determination. *Acta Crystallogr.* **2015**, *71*, 3−8. (b) Sheldrick, G. M. Crystal structure refinement with SHELXL. *Acta Crystallogr.* **2015**, *71*, 3−8.
(54) Nonius B V. *"Collect" Data Collection Software*, 1998. (b) "Scalepack" data processing software: Otwinowski, Z.; Minor, W. Processing of X-ray diffraction data collected in oscillation mode. *Methods in Enzymology*; Macromolecular Crystallography, Part A; Academic Press, 1997; Vol. *276*, pp 307−326.
(55) Cromer, D. T.; Waber, J. T. *International Tables for X-ray Crystallography*; Ibers, J. A., Hamilton, W. C., Eds.; Kynoch: Birmingham, England, 1974.
(56) Spek, A. L. *PLATON—A Multipurpose Crystallographic Tool*; Utrecht University: Utrecht, Netherlands, 2003.
(57) Flack, H. D. On Enantiomorph-Polarity Estimation. *Acta Crystallogr., Sect. A: Found. Crystallogr.* **1983**, *39*, 876−881.

https://doi.org/10.1021/acs.organomet.1c00708
Organometallics 2022, 41, 733−749